Check for updates

JGR Space Physics

RESEARCH ARTICLE
10.1029/2022JA030771

Special Section:
The Demonstration and Science Experiment Satellite: Instruments and Mission Overview

Overview of the Demonstration and Science Experiments (DSX) Mission

W. R. Johnston[1], G. P. Ginet[2], M. J. Starks[1], J. P. McCollough[1,3], J. C. Sanchez[1,4], P. Song[5], I. A. Galkin[5], U. S. Inan[6,7], D. S. Lauben[6], J. Tu[5], B. W. Reinisch[5,8], I. R. Linscott[6], K. Roche[5], S. Stelmash[5], S. Allgeier[2], R. Lambour[2], J. Schoenberg[2], W. Gillespie[2], W. M. Farrell[9], M. A. Xapsos[9], P. A. Roddy[1], C. D. Lindstrom[1], G. F. Pedinotti[10,11], S. L. Huston[12], J. M. Albert[1], A. J. Sinclair[1], L. D. Davis[13], J. A. Carilli[1], D. L. Cooke[1], and C. W. Parker[14]

[1]Air Force Research Laboratory, Space Vehicles Directorate, Kirtland AFB, NM, USA, [2]Massachusetts Institute of Technology Lincoln Laboratory, Lexington, MA, USA, [3]Now at U.S. Department of Energy, Albuquerque, NM, USA, [4]Now at Space Systems Command, Kirtland AFB, NM, USA, [5]Space Science Laboratory, University of Massachusetts Lowell, Lowell, MA, USA, [6]Department of Electrical Engineering, Stanford University, Palo Alto, CA, USA, [7]Department of Electrical Engineering, Koç University, Istanbul, Turkey, [8]Lowell Digisonde International, LLC, Lowell, MA, USA, [9]Goddard Space Flight Center, National Aeronautics and Space Administration, Greenbelt, MD, USA, [10]ATA-Aerospace, Albuquerque, NM, USA, [11]Now at Axient, Albuquerque, NM, USA, [12]Confluence Analytics, New Bern, NC, USA, [13]SRC, North Syracuse, NY, USA, [14]Applied Physics Laboratory, John Hopkins University, Laurel, MD, USA

Abstract The Air Force Research Laboratory's Demonstration and Science Experiments (DSX) mission investigated wave-particle interactions and the particle and space environment in Medium Earth Orbit (MEO) from June 2019 to May 2021. Its Wave-Particle Interactions Experiment conducted over 1,300 active high power very low frequency transmissions in the radiation belts providing observations of antenna performance and signal propagation from a controlled source. This included hundreds of transmissions while in magnetic conjunction with other satellites. The Loss Cone Imager and Space Weather Experiment suite observed electron and proton populations over a wide energy range, with several of these instruments providing pitch-angle resolution. The Space Environmental Effects Experiment investigated effects of the MEO environment on electronics and materials. The Adaptive Controls Experiment demonstrated technology for on-board identification and control of large structure vibrational modes. We describe the DSX instrument capabilities and on orbit performance, science planning and operations for carrying out an array of active and passive experiments, and some initial results in brief. We also describe plans for further work and data release.

Plain Language Summary In this paper, we summarize the Air Force Research Laboratory's Demonstration and Science Experiments (DSX) satellite mission which recently concluded after nearly 2 yr in the radiation belts. We describe the DSX science instruments and how we planned and performed experiments during the mission. The mission had a primary goal of conducting high-power transmissions in near-Earth space using very low frequency (VLF) radio waves. Such active DSX experiments yielded information about how a high-voltage antenna interacts with the low-density charged particles, or plasma, near the spacecraft. DSX experimented with propagating signals along magnetic field lines to other satellites and "bouncing" them back to the spacecraft. DSX also studied interactions between VLF waves and radiation belt electrons, particularly how electrons may be lost from the radiation belts. High-energy electrons and protons trapped in the Earth's magnetic field make up the radiation belts, and these particles as well as the lower-energy plasma particles are hazards to spacecraft. The mission had further goals of measuring radiation belt and plasma particles and their effects on spacecraft parts. Collectively, the results of DSX research will improve spacecraft survivability in the harsh space environment.

Key Points:

- Demonstration and Science Experiments conducted over 1,300 high power very low frequency transmission experiments in the radiation belts, including 315 in coordination with other satellites
- The 23-month mission also collected comprehensive wave, particle, and plasma observations in its inclined medium Earth orbit
- Instruments, planning and operations, some initial results, plans for further work, and release of data are described in brief

Supporting Information:

Supporting Information may be found in the online version of this article.

Correspondence to:

W. R. Johnston,
ae9ap9@vdl.afrl.af.mil

Citation:

Johnston, W. R., Ginet, G. P., Starks, M. J., McCollough, J. P., Sanchez, J. C., Song, P., et al. (2023). Overview of the Demonstration and Science Experiments (DSX) mission. *Journal of Geophysical Research: Space Physics*, *128*, e2022JA030771. https://doi.org/10.1029/2022JA030771

Received 5 JUL 2022
Accepted 20 NOV 2022

© 2023 The Authors. This article has been contributed to by U.S. Government employees and their work is in the public domain in the USA.
This is an open access article under the terms of the Creative Commons Attribution License, which permits use, distribution and reproduction in any medium, provided the original work is properly cited.

1. Introduction

The Demonstration and Science Experiments (DSX) spacecraft, operated by the Air Force Research Laboratory (AFRL), was launched on 25 June 2019 into Medium Earth Orbit (MEO; 6,000 km x 12,000 km × 42°, 5.3 hr period) and operated through 31 May 2021. Its primary science objective was to conduct unique high-power very low frequency (VLF) transmissions in the radiation belts to study wave-particle interactions. Such interactions are a major driver of radiation belt dynamics (e.g., Abel & Thorne, 1998; Kennel & Petschek, 1966;

21699402, 2023, 4, Downloaded from https://agupubs.onlinelibrary.wiley.com/doi/10.1029/2022JA030771 by Koc University, Wiley Online Library on [19/02/2025]. See the Terms and Conditions (https://onlinelibrary.wiley.com/terms-and-conditions) on Wiley Online Library for rules of use; OA articles are governed by the applicable Creative Commons License

W. Li & Hudson, 2019; Lyons & Thorne, 1973) and have been the subject of intense study for decades by active ground-based wave injections (Carpenter et al., 1997; Golkowski et al., 2019; Helliwell, 1988; Helliwell & Katsufrakis, 1974; Imhof et al., 1983; J. D. Li et al., 2015; Sonwalkar et al., 1997) and by passive space-based experiments (e.g., Baker & Blake, 2012; Brautigam, 2002; Kanekal et al., 2019; Miyoshi et al., 2018) but DSX conducted the first space-based active experimentation with high power transmissions.

This paper first provides the historical background of the DSX mission and an overview of the spacecraft. This is followed by a description of the four top-level experiment suites including their science objectives and associated instruments. Next, the mission planning concept and process are discussed with focus on how this accommodated a high cadence of active high-power VLF transmission experiments. Results are summarized in terms of experiment performance and data collection, scientific analysis to date, and on-going work. Data availability is then addressed and overall conclusions given.

2. Background of DSX Mission

DSX was originally proposed by AFRL researchers in 2003 and selected as the fourth AFRL space science technology experiment (SSTE-4) in 2004. It was initially conceived as the Deployable Structures Experiment (DSX) with investigations of (a) aspects of large deployable space structures including antennas and solar arrays, (b) wave-particle interactions in the radiation belts, (c) performance and degradation of thin-film photovoltaics in MEO, and (d) energetic particle and plasma populations in MEO. The initial spacecraft baseline included a VLF receive-only antenna, intended for use in conjunction with ground-based VLF transmitters. Subsequently, a high-power VLF transmitter was added, the large roll-out solar array was eliminated, and the mission was renamed Demonstration and Science Experiments (maintaining the DSX acronym). The experimental objectives became the current ones of (a) investigating wave-particle interactions in the radiation belts using a high-power space-based VLF transmitter, (b) mapping the energetic particle and plasma environment in MEO, (c) investigating MEO environment impacts on materials and components, and (d) experimenting with active control of a large space structure. Besides adding a VLF transmitter and increasing the antenna length, the space weather particle instrument suite was increased from four to five instruments. For more background see Easley et al. (2004), Scherbarth et al. (2009), and Schoenberg et al. (2006).

Transition of DSX into an active experiment for investigating VLF wave-particle interactions took advantage of the fact that the original plans for a large structure would enable long antennas for VLF transmissions. This allowed DSX to explore potential technologies for space-based radiation belt remediation (RBR), that is, injecting VLF waves into an artificial radiation belt that might result from a high-altitude nuclear detonation in order to enhance particle loss rates and reduce damage to space assets (Carlsten et al., 2019; Winter et al., 2004). Such artificial belts were produced following high-altitude nuclear tests in 1958–1962, sometimes persisting for years with significant impacts on then-operating satellites (Gombosi et al., 2017). The modern proliferation of satellites in low-Earth orbit (LEO) and associated services for both military and civilian applications has high vulnerabilities to such an artificial belt, leading to U.S. DoD pursuit of RBR technologies.

Space-based radio wave transmissions for environmental observation applications have been performed in the past, though there are limited examples at VLF frequencies (3–30 kHz) due to non-line-of-sight propagation and large required antenna lengths. In 1989–1990 the Activny spacecraft made several VLF transmissions during conjunctions with Dynamics Explorer 1 though no remote detections were observed (Sonwalkar et al., 1994). NASA's Imager for Magnetopause-to-Aurora Global Exploration (IMAGE) mission (Burch, 2000) conducted very-low to medium frequency (MF) transmissions in 2000–2005 using the Radio Plasma Imager (RPI) instrument (Reinisch et al., 2000). RPI was focused on remote sensing of plasma structures by transmitting at frequencies from 3 kHz to 3 MHz and observing subsequent signal reflection from within the magnetosphere, plasmasphere, or ionosphere. Though RPI was not optimized for low frequency (LF) transmissions and consequently limited in power in the VLF range, it nonetheless demonstrated signal propagation and efficient reflection mechanisms within the magnetosphere and at the Earth-ionosphere boundary for round trip distances exceeding 10,000 km (Sonwalkar et al., 2004, 2011; Sonwalkar, Reddy, & Carpenter, 2011). These experiments also showed that RPI/IMAGE radiated sufficient power at VLF at small and large (close to resonance cone) wave normal angles to be detectable at the satellite after long-distance round trip propagation. RPI experiments further demonstrated key engineering parameters for a space-based VLF transmitter (Paznukhov et al., 2010; Song et al., 2007). The DSX program was pursued with a high-power VLF transmitter and a broadband VLF receiver because such a

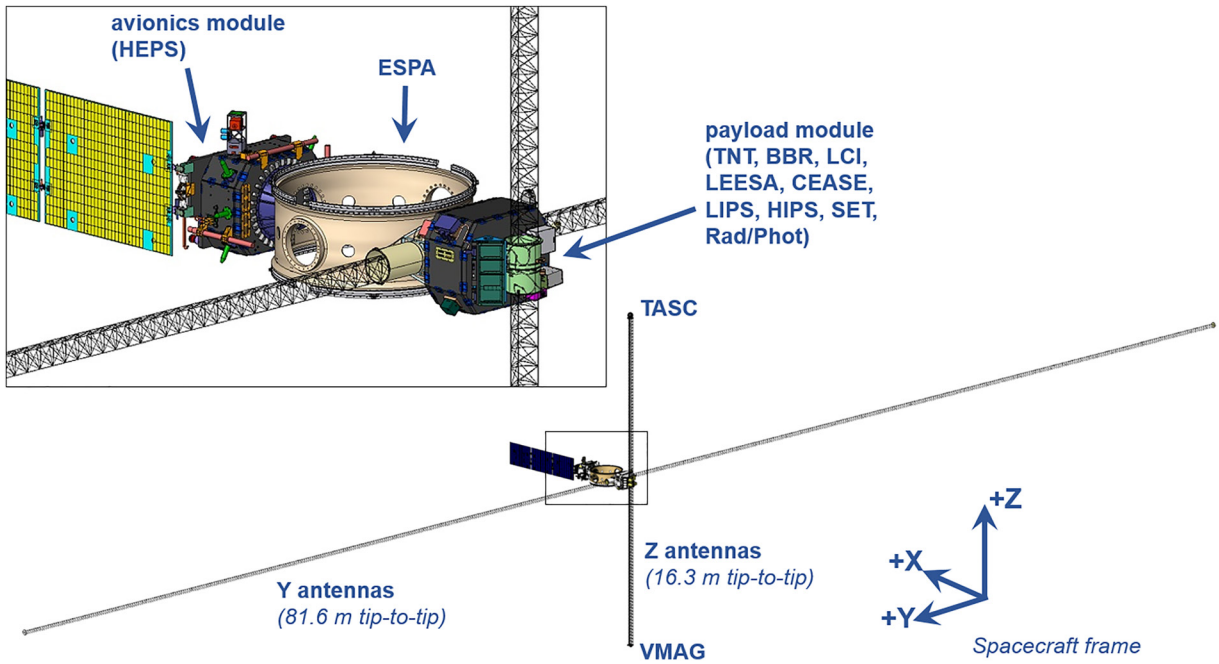


Figure 1. Deployed configuration of the Demonstration and Science Experiments spacecraft and the location of the science instruments, with upper left inset showing avionics and payload modules. Spacecraft coordinate axes indicated at lower right.

transmitter and receiver were required in situ to determine both the efficiency of near-field wave injection and far-field propagation.

The DSX spacecraft was the first spacecraft designed with an Evolved Expendable Launch Vehicle Secondary Payload Adapter (ESPA) Ring as the primary structure. The ESPA ring is designed to fit between the primary payload and second stage of a launch vehicle, facilitating addition of payloads that can take advantage of excess margin on large satellite launch vehicles. The DSX satellite is composed of a payload module and an avionics module attached to an ESPA ring. Figure 1 illustrates the spacecraft in a deployed configuration including locations of science instruments, which are described in the following section. Extending from the payload module are two sets of booms: one pair in the $\pm Z$ direction with each deployed boom of length 8 m yielding a 16.3 m tip-to-tip length when the payload module height is included; and the other pair in the $\pm Y$ direction with each deployed boom of length 40 m yielding a tip-to-tip length of 81.6 m when the payload module width is included. The booms support the electric field (*E*-field) transmit antenna (*Y* boom), the *E*-field receiver antennas (*Y* and *Z* booms), the three-axis AC search coil magnetometer (tip of the $+Z$ boom) and the three-axis DC Vector Magnetometer (VMAG; tip of the $-Z$ boom). DSX had no propulsion but did have three-axis attitude control which, given its semi-rigid antennas, enabled manipulation of antenna orientation with respect to the geomagnetic field.

DSX was initially planned for launch as early as 2008 with Defense Meteorological Satellite Program Flight-19 (DMSP F-19) but was later switched to a planned launch on DoD's Space Test Program 2 (STP-2) mission, which experienced delays before finally launching in June 2019 aboard a SpaceX Falcon Heavy.

3. DSX Science Experiment Suites

3.1. Wave Particle Interactions Experiment

The Wave Particle Interaction Experiment (WPIx) explored the injection, propagation, amplification, and natural distribution of VLF waves in the magnetosphere. Questions addressed included the radiation pattern, sheath effects on antenna impedance, linear and nonlinear amplification, and the generation of triggered emissions (Ginet, 2020; Song et al., 2021). It further explored the interaction of such VLF waves with trapped radiation belt electrons, particularly resonance-induced losses of such particles. This was principally accomplished by conducting high-power VLF transmissions in the MEO region and measuring transmitter parameters, observing propagation and other plasma interactions induced by these waves, and looking for effects on trapped electrons.

21699402, 2023, 4, Downloaded from https://agupubs.onlinelibrary.wiley.com/doi/10.1029/2022JA030771 by Koc University, Wiley Online Library on [19/02/2025]. See the Terms and Conditions (https://onlinelibrary.wiley.com/terms-and-conditions) on Wiley Online Library for rules of use; OA articles are governed by the applicable Creative Commons License

21699402, 2023, 4, Downloaded from https://agupubs.onlinelibrary.wiley.com/doi/10.1029/2022JA030771 by Koc University, Wiley Online Library on [19/02/2025]. See the Terms and Conditions (https://onlinelibrary.wiley.com/terms-and-conditions) on Wiley Online Library for rules of use; OA articles are governed by the applicable Creative Commons License

Table 1
Properties of Demonstration and Science Experiments (DSX) Electric and Magnetic Field Instruments

Instrument	Type	Measured quantities	Measurement range	Recording cadence	Sensitivity
TNT	Dipole antenna	AC electric fields, plasma density	3–750 kHz (receive) 3–50 kHz (transmit) 66 dB (receive) 5 kV nominal, 10 kV end of life (transmit) 1.1×10^6 m^{-3}–7×10^9 m^{-3} (derived plasma density)	7 s (receive) 300 s (plasma density)	2.5×10^{-17} V^2/Hz (receive)
BBR/TASC	Two dipole antennas (*E*-field); 3 magnetic search coils (*B*-field)	AC electric and magnetic fields	100 Hz–50 kHz broadband 90 dB spurious free dynamic range	30 s (spectrogram) 1 s (multiband)	1.0×10^{-16} V^2/m^{2}Hz at 7 kHz (*E*-field) 1.0×10^{-11} nT^2/Hz at 7 kHz (*B*-field)
VMAG	One vector fluxgate magnetometer	Magnetic field	DC-10 Hz ±10,000 nT	0.05 s	<0.1 nT

DSX was required to conduct statistically significant numbers of high-power transmission experiments exploring variation of parameters including transmission power and frequency, pulse patterns, antenna orientation relative to local magnetic field, and local magnetic field and plasma conditions. Further information was added by coordinated remote observations of transmitted VLF waves as well as possible particle effects, requiring joint planning of conjunction experiments with other missions. The WPIx instrument suite comprised the Wave Induced Precipitation of Electron Radiation (WIPER) transmitter and receiver, the VMAG, and an electron loss cone detector as described below.

The WIPER package includes: the Tuner Control Unit (TCU), NarrowBand Receiver (NBR), and Transmitter Amplifier and Tuner Unit (TATU), collectively called TNT and built by the University of Massachusetts Lowell; the BroadBand Receiver (BBR) built by Stanford University; and the Tri-Axial Search Coil (TASC) built by NASA/Goddard Space Flight Center. These components utilized the two antennas, the 81.6 m tip-to-tip dipole *Y* antennas and the 16.3 m tip-to-tip dipole *Z* antennas. Collectively these components permit the following experiments: high power transmissions at VLF frequencies and reception of return signals; low power sounding transmissions with reception of return signals; and passive VLF surveys. Properties of the WPIx instruments are summarized in Table 1.

Among TNT components, TATU is a pair of broadband VLF/LF/MF transmitters capable of operating at combined power up to ∼1 kW at frequencies between 3 and 50 kHz in the high-power transmission mode, and less than 1 W at frequencies between 50 and 750 kHz for the relaxation sounding mode. NBR is a narrowband electric field VLF/LF/MF receiver covering the band from 3 to 750 kHz. The TCU is a pair of tuners that adaptively maximize antenna current under different plasma conditions. TNT is coupled to the 81 m antennae mounted on the ±*Y* booms for transmissions.

TNT design was informed by experience with design and operation of the IMAGE RPI instrument (Reinisch et al., 2000). Transmissions with an electrically short dipole face two challenges: first, a very high driving voltage is required to produce sufficiently high current into the antenna because the antenna impedance is mainly capacitive, and second, the radiation efficiency is very poor at low frequencies. Since safe operation of RPI limited its antenna input voltage to 1.5 kV, transmitted power could not reach much higher than 1 mW in VLF bands. For TNT, nominal input voltage was 5 kV and operating power up to ∼1 kW (radiated power for TNT is still being assessed).

The TNT instrument was required to handle highly stressful operations given that it would perform adjustable, tuned, high-power transmissions (Reinisch et al., 2022). Each TATU included two power units. The TATUs could execute diverse transmission sequences, programmable on orbit, including fixed or tuned frequency transmission pulses of varying lengths and frequency patterns, including pauses for listening/receive periods. The adaptive tuning capability of the TCU included both software and hardware fuses to prevent overvoltage or overcurrent states.

21699402, 2023, 4, Downloaded from https://agupubs.onlinelibrary.wiley.com/doi/10.1029/2022JA030771 by Koc University, Wiley Online Library on [19/02/2025]. See the Terms and Conditions (https://onlinelibrary.wiley.com/terms-and-conditions) on Wiley Online Library for rules of use; OA articles are governed by the applicable Creative Commons License

Table 2
Properties of Demonstration and Science Experiments (DSX) Particle Instruments

Instruments	Type	Electron channels	Proton channels	Field of view (full angle/ width)	Time sampling	Geometric factor (cm^2 sr)
CEASE	Telescope + 2 dosimeters	>0.13 to >3.5 MeV, 9 channels	>16 to >79 MeV, 12 channels	90° FOV (tel), 180° FOV (dos), same look directions	5 s	0.00096–0.36 (electrons); 0.0079–1.16 (protons)
LEESA	Programmable ESA	Tens of eV to 30 keV, up to 256 energies	Tens of eV to 30 keV, up to 256 energies	Five pixels, 120° × 12° total FOV	12.5 or 125 ms/ sample	~0.01 (electrons); ~0.015 (protons)
LIPS	Scintillator pixels	60 keV to >2 MeV, ~5 channels	60 keV to >2 MeV, ~5 channels	Eight pixels, 79° × 8° total FOV	1 s	0.0001
HIPS	Pixelated telescope	1.1–12 MeV, 5+ channels	14–300 MeV, 9 channels	Eight pixels, 90° × 12.5° total FOV	1 s	0.002
HEPS	Telescope	Four channels	20–440 MeV, 23 channels	15°–25° FOV	10 s	0.01–0.04 (protons)
LCI-FSH	Three pixelated telescopes	30–550 keV, 5 channels	No	Eighteen pixels, 180° × 10° total FOV	500, 167, or 50 ms	0.001
LCI-HST	Telescope	30–850 keV, 4 channels	350–850 keV, 1 channel	14° FOV	500, 167, or 50 ms	0.1

The BBR is a sensitive analog vector wave receiver for whistler mode signals in the VLF range. The BBR accepts electric wave signals from the 16 m ± Z dipole antenna and also the 81 m ± Y antenna via the TNT electronics. The BBR also accepts magnetic wave signals from the TASC magnetometer mounted on the DSX + Z boom. TASC consists of three highly sensitive orthogonal magnetic search coils and front-end preamplifiers that measure from 100 Hz to 50 kHz and is mounted on the end of the 8 m + Z boom. Full-resolution BBR data is too voluminous for download from the spacecraft when recorded for more than 30 s, so it is processed on-board by the Software Receiver (SRx) program run on the spacecraft's Experimental Computer System. SRx yielded a number of time-domain and frequency domain data products for download.

The VMAG was built by the University of California-Los Angeles to measure the three-dimensional DC magnetic field (Moldwin, 2010). VMAG measures the geomagnetic field from 100 to 10,000 nT over a frequency range of 0–10 Hz with a sensitivity of 0.1 nT and a field vector accuracy of <1°. VMAG is considered a DC magnetometer since it has a limited frequency range (when compared to the TASC magnetometer that measures from 100 Hz to 50 kHz). VMAG is located on the end of the 8 m -Z boom and consists of an electronics unit, a sensor head assembly, and a sensor cable assembly.

The Loss Cone Imager (LCI), built by Boston University, was designed to observe the ambient energetic electron environment as well as electrons scattered by VLF waves, either ambient or transmitted by DSX. It has two components, the High Sensitivity Telescope (HST) and Fixed Sensor Head (FSH). The LCI HST is a three-element particle telescope with anti-coincidence solid state detector (SSD) and collimator, yielding a large geometric factor (0.1 cm^2 sr) for sensing the small electron fluxes within the local loss cone, or the direction in which particle trajectories are no longer trapped. It has a 14° field of view (FOV) plus shielding to support loss cone observations while minimizing contamination from trapped particles. The LCI FSH is composed of three identical telescopes, each with a 60° × 10° field-of-view. Each telescope includes a pinhole aperture and six SSD pixels. The three telescopes are arranged on the FSH to create a combined FOV of 180° × 10°. LCI is mounted such that when the HST is viewing the loss cone, the FSH samples the full local pitch angle distribution. For more information see Carssow et al. (2009), Parker et al. (2016, 2009, 2014), Sullivan (2009), and Voss et al. (2009). Table 2 gives summary characteristics of LCI (along with the Space Weather Experiment [SWx] particle instruments described below).

3.2. Space Weather Experiment

The objective of the SWx was to obtain particle flux observations in the MEO regime including protons and electrons over energies ranging from plasma to relativistic particles. Applications include: diagnosing particle hazard climatologies in MEO to contribute to improvements of AFRL's International Radiation Environment Near Earth

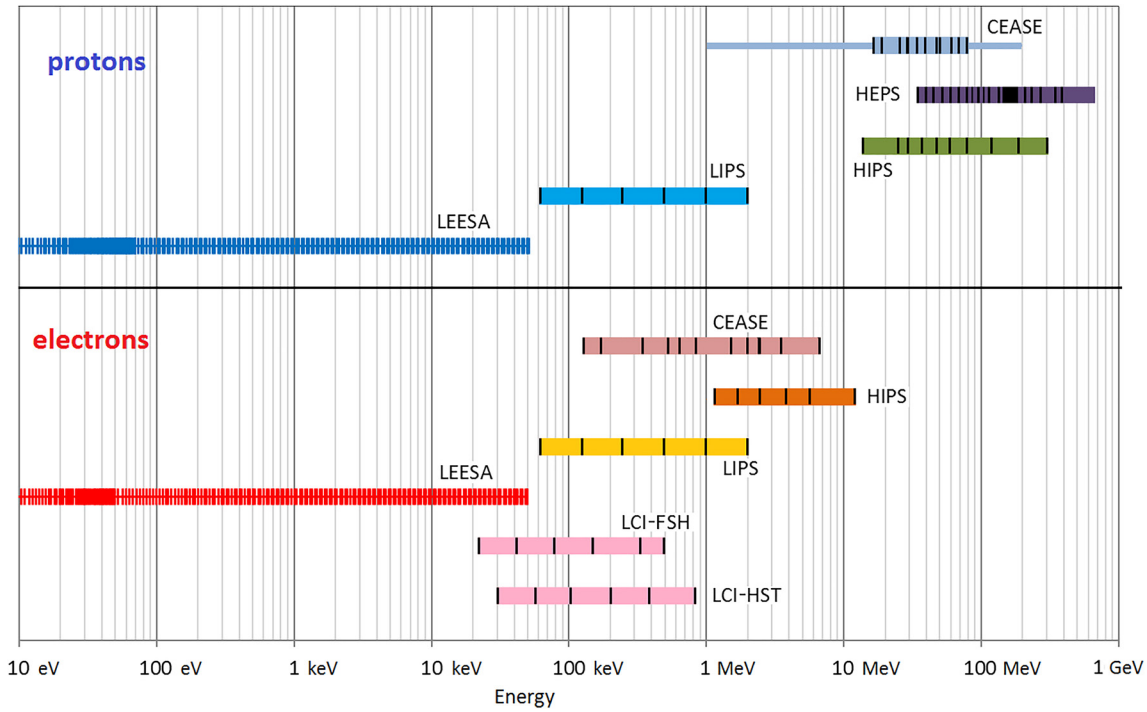


Figure 2. Energy coverage for Demonstration and Science Experiments particle instruments. Colored segments between black lines show standard channel boundaries, the thin line for Compact Environmental Anomaly Sensor (CEASE) protons shows additional logic bin energy responses, and the fine lines for Low Energy Electrostatic Analyzer (LEESA) show all energies potentially sampled.

(IRENE) model suite for applications including spacecraft design (Ginet et al., 2013; Johnston et al., 2015); diagnosing the ambient environment for active WPIx experiments; and providing observations in support of basic science research on dynamics of the radiation belts in MEO, given that this is a highly dynamic region. The DSX orbit in MEO sampled a more limited region of the radiation belts than missions such as Combined Release and Radiation Effects Satellite (CRRES), Van Allen Probes, or Arase and had a shorter orbital period than these missions. This resulted in a higher cadence of sampling and more coverage in local time and magnetic latitude, both particularly valuable for plasma observations.

The SWx package included five instruments to observe plasma and particle fluxes from tens of eV to 12 MeV for electrons and tens of eV to 440 MeV for protons, summarized in Figure 2 (Fennelly, 2009). All are mounted on the outside surface of the payload module with the exception of the High Energy Proton Spectrometer (HEPS), which is mounted on a tower on the avionics module. Three of these instruments have multiple look directions and for typical spacecraft orientation during high-power transmissions their look directions permitted surveys of the full local pitch angle distribution. Table 2 summarizes the properties of these instruments with further descriptions in the following paragraphs.

The Compact Environmental Anomaly Sensor (CEASE) instrument measured charged particles responsible for four primary hazards associated with the space radiation environment, that is, radiation dose, dose rate, deep dielectric charging, and single event effects (SEEs). The unit flown on DSX was built by Amptek, Inc., and tested and delivered by Assurance Technology Corp. It measured protons from 20 to 100 MeV and electrons from 11 keV to 6.5 MeV. Reported data include 36 logic bins including the nine electron and 12 proton standard integral channels, though a number of these channels respond to both species. Reported logic bins respond to total energy ranges of 45 keV–10 MeV for electrons and 0.9–90 MeV for protons. CEASE measures these particles with four radiation sensors: two dosimeters (with differing shielding), a particle telescope comprising two SSDs, and an SEE monitor. The telescope and dosimeters have parallel look directions with full angle conical FOVs of 60° and 90°, respectively. For more information see Brautigam (2008), Dichter, McGarity, Mullen, Brautigam, and Galica (2009), and Dichter et al. (1998).

CEASE units have flown on five missions prior to DSX. These include both CEASE 1 and CEASE 2 instruments, which are identical other than excluding or including an electrostatic analyzer (ESA), respectively; the

21699402, 2023, 4, Downloaded from https://agupubs.onlinelibrary.wiley.com/doi/10.1029/2022JA030771 by Koc University, Wiley Online Library on [19/02/2025]. See the Terms and Conditions (https://onlinelibrary.wiley.com/terms-and-conditions) on Wiley Online Library for rules of use; OA articles are governed by the applicable Creative Commons License

21699402, 2023, 4, Downloaded from https://agupubs.onlinelibrary.wiley.com/doi/10.1029/2022JA030771 by Koc University, Wiley Online Library on [19/02/2025]. See the Terms and Conditions (https://onlinelibrary.wiley.com/terms-and-conditions) on Wiley Online Library for rules of use; OA articles are governed by the applicable Creative Commons License

DSX CEASE unit is a CEASE 1. (These are to be distinguished from CEASE 3, a new design by AFRL first flown in 2021.) The prior flight heritage made CEASE the best characterized of DSX particle instruments and a baseline for intercalibration. Prior work with CEASE data has enabled spectral inversions using logic bins additional to the standard proton channels, which for appropriate energy spectra yields proton fluxes down to 1–5 MeV.

The Low Energy Electrostatic Analyzer (LEESA) measured electron and ion fluxes for relatively low particle energies, those responsible for surface charging and damage to thin films. Amptek, Inc., initiated work on a design derived from that of the Special Sensor J (SSJ) particle instruments flown on DMSP. Later AFRL took over the project and completed design changes and fabrication of the unit. LEESA measured particles in energy levels ranging from 30 eV to 50 keV in 256 log-spaced steps (or a subset thereof). It comprises two pairs of concentric quarter spherical ESAs. Equal sized apertures permit entry of electrons and ions between the analyzers, with the analyzers cycled through a series of voltages allowing particles of a limited energy range to travel between the spherical sections and reach the detector plane. During each cycle 80 energies are sampled, each of which is selectable from 256 energy values; the choices and sequence of energies are described by programs which may be selected and reprogrammed. This flexibility allows for prompt transition among programmed survey modes, plus the ability to change these survey modes on orbit. The instrument FOV is 120° × 12°, covered by five angular zones each for electrons and ions. LEESA is designed to operate at two different data rate levels, high and low; the low data rate is the normal operating mode, while the high data rate is used in support of DSX TNT operations. During high-power transmissions, LEESA measured electrostatic sheath dynamics and local plasma heating and thus is considered part of WPIx during these experiments (Mandell et al., 2019).

The Low-energy Imaging Particle Spectrometer (LIPS), built by Physical Sciences, Inc., observed electrons and protons of energies from 60 keV to >2 MeV for both species. Separate detectors for the two species each comprise a pinhole aperture limiting particle access to eight detector pixels. Each detector pixel includes a light block/particle discriminator layer, a plastic scintillator layer, and a photomultiplier tube. LIPS measured both electrons and protons in eight equally spaced angular bins having a combined FOV of 8 × 79°.

The High-energy Imaging Particle Spectrometer (HIPS), built by Physical Sciences, Inc., was intended to measure protons with energies between 30 and 300 MeV and electrons with energies between 1 and 10 MeV. HIPS is comprised of three detectors plus an anti-coincidence scintillator detector. The detectors include an SSD, a second segmented SSD (the 16 segments providing angular resolution) and a scintillator. Full FOV is a 12.5° × 90° fan divided into eight angular regions. HIPS did not report meaningful data from the beginning of the mission.

The High Energy Particle Spectrometer (HEPS) measured high-energy protons with energies from 20 to >440 MeV and electrons from 1.5 to 30 MeV (Dichter et al., 2009). It was designed and built by Amptek, Inc., and delivered by Assurance Technology Corp. The detector module is a particle telescope with four silicon detectors, two scintillator detectors, and an anti-coincidence scintillator detector plus passive shielding. A separate processing module performed processing of particle detections into the data stream. Counts were sorted into 120 logic bins for each of six logic masks. Data for all these logic bins were downloaded, with the standard 23 proton channels formed from a subset of these bins. It has one conical FOV of 15°–24° full angle depending on particle species and energy.

3.3. Space Environmental Effects Experiment

DSX hosted the SFx to measure aspects of the space environment and their impacts upon various spacecraft components and materials. The SFx instrument suite includes the Space Environment Testbed (SET) and the Radiometer and Photometer experiment.

The SET Project is part of the Living With a Star (LWS) Program managed at NASA Goddard Space Flight Center. The LWS Program, and the SET Project, is sponsored by NASA Headquarters Science Mission Directorate. Data from SET-1 on DSX will improve engineering approaches to accommodate and/or mitigate the effect of solar variability on space vehicle design and operations. It also reduces the risk for new technologies infused into future space missions and provides a standard mechanical, electrical, and thermal interface for a collection of small flight investigations. For more information see Fowler et al. (2004).

The SET-1 payload included the Cosmic Radiation Environment Dosimetry and Charging Experiment (CREDANCE) and the Central Carrier Assembly (CCA). CREDANCE is the Correlative Environment Monitor on

21699402, 2023, 4, Downloaded from https://agupubs.onlinelibrary.wiley.com/doi/10.1029/2022JA030771 by Koc University, Wiley Online Library on [19/02/2025]. See the Terms and Conditions (https://onlinelibrary.wiley.com/terms-and-conditions) on Wiley Online Library for rules of use; OA articles are governed by the applicable Creative Commons License

SET-1 and measures energetic proton flux at >40 MeV; linear energy transfer spectrum of solar and cosmic ions; internal charging current due to energetic electrons; and total ionizing dose. The CCA consists of:

- DIME-1 and DIME-2: Dosimetry Intercomparison and Miniaturization Experiments. These characterized the radiation environments for total ionizing dose and SEEs through the use of microdosimetry techniques with commercial-off-the-shelf (COTS) microelectronics requiring minimal space or weight.
- ELDRS: Enhanced Low Dose Rate Sensitivity in bipolar junction transistors. This measured gradual changes of transistor current within bipolar transistors manufactured in a COTS technology line. ELDRS characterized the base and collector currents of 24 COTS bipolar junction transistors as a function of emitter and gate voltages. These current-voltage relationships in turn enable characterization of low-dose rate (primary) and proton (secondary) effects in the space environment.
- COTS-2: Commercial Off-The-Shelf experiment for SEE mitigation. This investigated the sensitivity of commercial Static Random Access Memory-based Field Programmable Gate Arrays (Virtex2) to Single Event Upsets.

The objective of the Radiometer and Photometer experiments, developed by AFRL, was to directly measure changes in optical transmission, thermal absorption and emission due to the MEO radiation environment. It performed coupon-level testing of specific developmental coatings intended for thin-film photovoltaics with these sensors. The radiometers observed changes in thermal control paint coefficients of heat gain/loss based on exposure and the photometers measured the effect of erosion from quartz windows and re-deposition of material onto nearby optics.

3.4. Adaptive Controls Experiment

The Adaptive Controls Experiment (ACE) was an experiment for development of onboard systems to actively control attitude dynamics of large spacecraft like DSX (Davis & Sinclair, 2020). It specifically sought to validate technologies for extending the attitude control system bandwidth for highly flexible spacecraft that have significant dynamic modes within the bandwidth of their Attitude Determination and Control Subsystem (ADCS). ACE involved system identification experiments, usage of the resulting models in automated control design, and controller evaluation experiments. Individual ACE experiments typically lasted a few hours. ACE utilized the DSX ADCS, including the inertial measurement unit and three reaction wheels. The goal of ACE was to demonstrate at least a 10x improvement in attitude control bandwidth, with a stretch goal to increase bandwidth 100x.

In addition to ACE, NASA/Jet Propulsion Laboratory provided the Phaeton Mast Dynamics Central Assembly (PCA; Michaels, 2011). This was an experiment to measure vibrations of the DSX structure, including aspects of initial deployment and vehicle aging, utilizing a small accelerometer.

4. DSX Mission Planning

4.1. Planning Concept

While most magnetospheric missions are dominated by passive surveys, the DSX mission involved sustained and frequent active transmission experiments interspersed among passive data collection. In combination with restrictive resource constraints (e.g., power, data storage/processing, thermal management, and mission duration), experiment scheduling considerations drove development of a science planning process integrating the use of specialized software planning tools. General types of science experiments or observations were associated with constraints on spacecraft location and orientation, use of the transmitter and receiver, nature of any required conjunction with other assets, etc. For these experiments specific planning was done in terms of data collection events (DCEs), described in the next section. Campaigns of similar DCEs were conducted during mission based on factors such as current experimental objectives or opportunities for conjunctions with other assets. Below we describe details of this planning process followed by discussion of aspects specific to conjunction experiments.

4.2. DCEs and Experiment Planning

In DSX science planning, DCEs were time periods having distinct instrument settings (e.g., operating states of transmitter, receiver, and any multi-mode particle instruments) and spacecraft attitude modes. DCEs thus

21699402, 2023, 4, Downloaded from https://agupubs.onlinelibrary.wiley.com/doi/10.1029/2022JA030771 by Koc University, Wiley Online Library on [19/02/2025]. See the Terms and Conditions (https://onlinelibrary.wiley.com/terms-and-conditions) on Wiley Online Library for rules of use; OA articles are governed by the applicable Creative Commons License

Table 3
Types of Data Collection Events

DCE type	Description	Operational constraints and modes
Transmit	High-power VLF transmission during spatial and/or magnetic conjunction with another satellite (or high-altitude balloon)	Conjunction and L value criteria met; spacecraft generally in LCET mode; special LCI/LEESA modes
Blind Transmit	High-power VLF transmission with no remote target	L value constraints met; spacecraft generally in LCET mode; special LCI/LEESA modes
Receive	Passive high-resolution receive while in magnetic conjunction with a ground transmitter or lightning source	Conjunction criteria met; spacecraft generally in LCET mode
Survey	Passive science collection at all other times	Spacecraft attitude generally optimized for power collection and thermal management or ground contact

correspond to distinct high power transmission experiments, dedicated VLF receive periods, and the passive surveys filling the remaining time. The mission planning tools captured many of these constraints and options, tracked resources such as power and data storage, and handled both automated and manual population of DCE schedules for selected mission periods. The WPIx science team input ranged from fine level control of particular DCEs to setting prioritization of DCE types for extended science campaigns. Table 3 lists types of DCEs and their associated operational constraints.

Transmission DCEs, including both Transmit and Blind Transmit DCEs (with and without a conjunction target, respectively), were typically limited to ∼0.5 hr duration per 5.2 hr orbit due to power constraints. Receive DCEs were coincidentally limited to ∼0.5 hr per orbit due to data processing and telemetry constraints. Transmit, Blind Transmit, and Receive DCEs were operated in a high-time resolution "burst mode", while at all other times, a low data-rate mode containing time-averaged electromagnetic field spectra from both the BBR and TNT receivers comprised the Survey mode.

Transmission periods were selected during each orbit to optimize scientific returns. Most DSX transmissions were performed within the plasmasphere where higher plasma densities (relative to outside the plasmapause) yield higher radiation resistance and hence more radiated power. Given that plasma conditions vary, TNT actively tuned to optimize for local plasma conditions. This tuning could produce undesirable instrument effects for rapid drops in plasma density, that is, if being applied while DSX is exiting the plasmapause. Since the plasmapause is a dynamic boundary not well predicted on the timescales of DSX experiment planning, high-power transmissions were generally restricted to locations highly likely to be either well inside the plasmapause ($L < 3.5$) or well outside ($L > 5.5$). (Note that this nominal plasmapause location applied only for experiment planning, not to science analyses.) An exception was in the event of extreme geomagnetic storms, when survey observations would replace transmissions, but geomagnetic storms were relatively rare during the DSX mission.

The ∼30 min per orbit transmission experiments (range 5–40 min) were typically planned to occur near equator crossings. Thus most transmissions were in the region of $L = 2$–3, with specific locations changing over the course of the mission as the orbit precessed (Figure 3). Some transmissions were conducted at other locations either for targeted conjunctions with other missions or for other investigations. Tuned transmissions were selected among three frequency ranges—low (1.4–8.5 kHz), medium (6.6–23.4 kHz), or high (10.6–39.4 kHz)—while fixed frequency transmissions were typically at a chosen frequency in the 2.8–28 kHz range. Transmission patterns generally used a series of steps in a small frequency range to facilitate identification of a signal by a VLF receiver (either at DSX or another satellite). Transmissions attempting to produce a signal in precipitated electrons would use a pulsing pattern with pulse periods suited to analysis by the chosen target detector. The LEESA and LCI payloads both employed higher time cadence modes during high-power transmissions. LEESA also had the ability to survey different sets of particle energies at these times, a capability utilized to a limited extent for exploring transmission-induced plasma sheath heating.

Each DCE had an associated spacecraft attitude mode. Most high-power transmissions were conducted in loss cone edge tracking (LCET) mode in which the $\pm Y$ antennas were perpendicular to the local magnetic field, the LCI-HST look direction was northward just inside the estimated local loss cone, and the $+Y$ axis (outward from solar array) was as close to sun pointing as possible. Experiments not using LCET mode included those during the antenna orientation survey (AOS) campaign where the antennas had specified angular offsets to the magnetic field during transmissions.

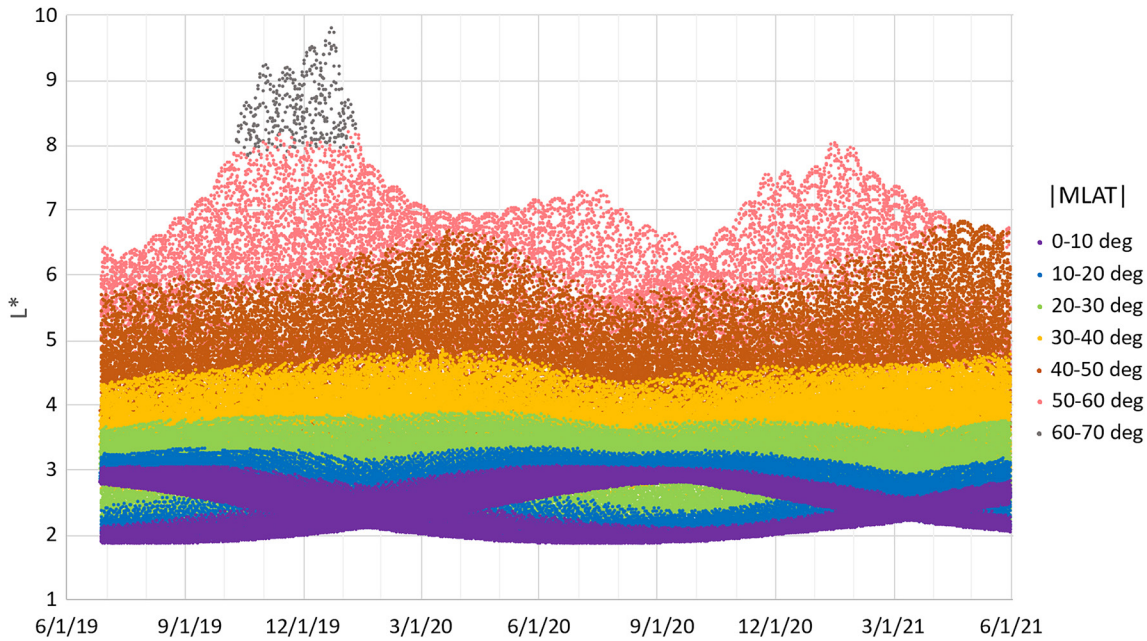


Figure 3. Demonstration and Science Experiments sampling in geomagnetic space over the full mission, with L^* plotted at 5 min intervals and color indicating magnetic latitude ranges.

Survey DCEs were planned for all time periods outside transmission or receive DCEs. The SWx and SFx instruments were generally operated in continuous data collection modes throughout the mission (including during transmission and receive DCEs), producing a long baseline for climatology and space environment effects studies. LEESA and LCI were operated in lower cadence modes during Survey periods. All particle instruments were mounted such that when the spacecraft was in LCET mode the instrument FOVs maximally sampled the local directional distribution of ambient particles. Most passive survey periods used sun track mode, optimizing spacecraft attitude for solar power collection, though particle instrument look directions were generally sub-optimal in this mode. Prior to launch the team discussed exploring compromise attitude modes that would improve particle data collection during passive survey periods. However, post-launch identification of thermal issues required a mix of sun track mode with "cold soak" attitudes (having a specified offset from sun-pointing) that provided for thermal management so improved pointing for passive survey was not pursued. Sun pointing had the $+Y$ axis pointed at the Sun and the Z axis as close as possible to parallel to the Earth's rotation axis, while cold soak offset the $+Y$ axis from sun pointing by a 60° rotation about the Z axis toward the $+X$ axis.

The high cadence of planned active experiments and their diversity required a streamlined approach to mission planning. Mission planning software tools were developed for this purpose. Primary among these was the "Gonzo" tool which would conduct orbit propagation, conjunction opportunity identification, and basic environment calculations. Then it would use a rules- and priorities-based system to initially populate experiments and downlink opportunities in a planning period. Constraints included experiment requirements, resources (e.g., data volume, on board processing, and power), and various conditions for conjunctions (both for active transmissions to other spacecraft and for passive reception from ground transmitters). Pre-mission exercises as well as operations on orbit demonstrated the need for additional manual inputs or adjustments to these plans, which were enabled in the tool via GUI. In this manner, transmit and receive DCEs would be scheduled with passive surveys filling the remaining time. In practice, DSX plans were developed for a week at a time, 1 week in advance, with daily adjustments to this plan as required, for example, for assigned downlink opportunities or changes from the science team. This planning timeline also provided for coordination with teams for conjunction targets, for example, communicating advance notice of planned times and frequencies for DSX transmissions. Output from the Gonzo tool plus additional intermediate tools captured operating states for payloads associated with each DCE, attitude requirements, etc., and ultimately produced command files.

On a broad scale the DSX mission included a number of overlapping campaigns. For high-power transmission experiments, the mission was planned to include an initial Learn to Transmit (L2Tx) campaign for initial

21699402, 2023, 4, Downloaded from https://agupubs.onlinelibrary.wiley.com/doi/10.1029/2022JA030771 by Koc University, Wiley Online Library on [19/02/2025]. See the Terms and Conditions (https://onlinelibrary.wiley.com/terms-and-conditions) on Wiley Online Library for rules of use; OA articles are governed by the applicable Creative Commons License

21699402, 2023, 4, Downloaded from https://agupubs.onlinelibrary.wiley.com/doi/10.1029/2022JA030771 by Koc University, Wiley Online Library on [19/02/2025]. See the Terms and Conditions (https://onlinelibrary.wiley.com/terms-and-conditions) on Wiley Online Library for rules of use; OA articles are governed by the applicable Creative Commons License

Table 4
List of Conjunction Assets for Demonstration and Science Experiments (DSX) Planning

Mission	Organization	Description	Launch date	Instrumentation (relevant to DSX exp.)	Number of DSX transmissions
Very Low-Frequency Propagation Mapper (VPM)	AFRL	One CubeSat, LEO (460 km, 52° inclin.)	1 February 2020	VLF receiver	80 (March–September 2020)
Arase (or ERG, Energization and Radiation in Geospace)	JAXA	One satellite, GTO (31° inclin.)	20 December 2016	VLF receiver and particle instruments	25 (August 2019 to May 2021)
Van Allen Probes (or RBSP, Radiation Belt Storm Probes)	NASA	Two satellites[a], GTO (11° inclin.)	30 August 2012	VLF receiver and particle instruments	8 (August–October 2019)
Focused Investigations of Relativistic Electron Burst Intensity, Range, and Dynamics 4 (FIREBIRD-4)	UNH/MSU	One satellite, polar LEO (420 × 570 km)	31 January 2015	Particle detector	31 (October 2020 to March 2021)
CAScade, Smallsat, and IOnospheric Polar Explorer (CASSIOPE)	CSA	One satellite, polar LEO (300 × 1,400 km)	29 September 2013	VLF receiver	158 (August 2019 to February 2021)
Balloon Array for Radiation-belt Relativistic Electron Losses (BARREL)	NASA	One balloon launch from Antarctica	7 January 2020	X-ray detector (for indirect particle detection)	20 (January–March 2020)
Polar Operational Environmental Satellites (POES) and METeorological Operational satellites (METOP)	NOAA/ESA	Six satellites, polar LEO (840 km)	Various	Particle detector	43 (August 2019 to December 2020)

[a]Only Van Allen Probes A operated during DSX science activities.

characterization of TNT followed by normal mission operations with various high-power transmissions, with a final "Hail Mary" campaign just prior to mission end in which maximum TNT driving voltages would be used. Conjunction opportunities for transmissions to other satellites generally varied over the course of the mission as the relative orbit orientations of DSX and a given target varied with respect to each other. These defined additional conjunction campaigns. Initial DSX mission concepts also involved significant periods of passive collection to characterize VLF from ground transmitters and lightning. By the time DSX launched, however, other satellites such as DEMETER and Van Allen Probes had acquired extensive observations of such VLF, allowing DSX to focus more on active experiments. The ACE experiments represented additional short campaigns as these experiments generally required a suspension of other experiments.

4.3. Conjunction Planning

Transmit DCEs with their associated conjunction constraints posed special planning requirements. During the mission, coordinated experiments were planned for conjunctions with 12 satellites and one balloon as listed in Table 4, with experiment types as follows:

- Radiation belt science missions with robust VLF and particle sensors and in orbits crossing the DSX orbit included Van Allen Probes (Mauk et al., 2013) and Arase (or ERG, Energization and Radiation in Geospace; Miyoshi et al., 2018). This enabled both geomagnetic and spatial conjunctions for joint experiments.
- LEO missions with VLF receivers included CASSIOPE (Yau et al., 2015) and VPM, with geomagnetic conjunction experiments possible for these spacecraft. VPM, or VLF Propagation Mapper (Marshall et al., 2021), was an AFRL CubeSat with objectives including coordinated VLF experiments with DSX.
- LEO missions with particle sensors included the POES/METOP constellation (Yando et al., 2011) as well as FIREBIRD-4 (Johnson et al., 2020). Experiments in this case involved DSX transmissions while in magnetic conjunction with the LEO spacecraft, allowing potential observation of electron precipitation induced by DSX transmissions.
- A high-altitude balloon launch in NASA's BARREL program (Millan et al., 2013) was targeted in one campaign, with BARREL detectors looking for X-rays resulting from electron precipitation induced by DSX.

Transmissions were not scheduled for conjunctions with ground receivers. DSX transmissions were expected to emit at low power and possibly with wave normals well off the geomagnetic field. Unless such signals were fortuitously entrained in a plasmaspheric duct, they would not be in the transmission cone (Helliwell et al., 1973)

21699402, 2023, 4, Downloaded from https://agupubs.onlinelibrary.wiley.com/doi/10.1029/2022JA030771 by Koc University, Wiley Online Library on [19/02/2025]. See the Terms and Conditions (https://onlinelibrary.wiley.com/terms-and-conditions) on Wiley Online Library for rules of use; OA articles are governed by the applicable Creative Commons License

at the topside ionosphere, and thus not penetrate to the ground. Scheduling these experiments would be difficult, as the ionospheric absorption is not known on any given day. Consequently, we focused on space-to-space and "boomerang" experiments to avoid these issues. Given the number and varied characteristics of transmissions performed, it is still possible that a small subset produced recordable signatures in ground receivers. Hence, with the release of our full list of transmissions (Section 5.4), comparisons with archived contemporaneous ground receiver data can be explored.

The DSX mission planning tools used spatial ephemerides for DSX and potential target spacecraft at a 1 min time resolution to identify two types of conjunctions: spatial and magnetic. Predicted spatial conjunctions were defined by physical separation between the two spacecraft of less than 2,000 km, while predicted magnetic conjunctions were identified when the target spacecraft came within 750 km in the plane normal to the geomagnetic field line traced from DSX, though the distance along the magnetic field can be large. The DSX field line was traced using the International Geomagnetic Reference Field (IGRF-12; Thébault et al., 2015) plus the Olson-Pfitzer quiet external field (Olson & Pfitzer, 1974, 1977) models both north and south from the predicted spacecraft location. Receive conjunctions were defined based on thresholds of estimated wave power from ground transmitters using models of VLF propagation from those sources (Lehtinen & Inan, 2009; Starks et al., 2020).

During the mission, offline identification of conjunctions was common either for types of conjunctions where the above criteria were inappropriate or where they were otherwise found to be inaccurate. For conjunctions with FIREBIRD-4, intended to allow potential observation of DSX transmission-induced electron precipitation at LEO, ray tracing was conducted for candidate conjunctions to identify high-quality opportunities as well as to select appropriate transmission frequencies for DSX. Ray tracing was also used to select frequencies and (later) identify opportunities for transmissions to VPM, accounting for VPM limitations requiring short data collects. Transmissions in conjunction with the BARREL balloon mission were challenging given the unpredictability of BARREL's wind-driven location multiple days in advance (per the DSX planning cycle). Geographic and geomagnetic criteria were used with extrapolations of the BARREL location to plan these experiments.

5. DSX Mission Results

5.1. Mission Summary

DSX was launched on 25 June 2019 as the last of 24 payloads deployed from the STP-2 Falcon Heavy launch. Antenna deployment was completed 12 July and payload commissioning was completed 13 August. The nominal 1 yr mission began with end of launch and early operations on 23 August 2019, but DSX was granted successive mission extensions to January and May of 2021. The mission ended with passivation of the spacecraft on 31 May 2021.

The "Learn-to-Transmit" (L2Tx) campaign began 23 August 2019, involving progression through initial TNT operations including ramp-up of driving voltage. L2Tx was declared complete on 12 April 2020 with the first confirmed "boomerang" detection, or reception of a DSX VLF signal back at DSX. In July 2020 a period of modified payload operations began to assess and improve transmitter performance. This included operations in asymmetric mode in September–October 2020, where only one of the two *Y* antennas was operated. Limited asymmetric operations occurred at later times in the mission as well. In January–April 2021 an AOS campaign was conducted, with selected transmissions conducted with the antenna at various angles to the local magnetic field, rather than the default of antenna perpendicular to the magnetic field.

As enumerated in the last column of Table 4, DSX campaigns of transmission experiments were conducted with other spacecraft throughout the mission as conjunction opportunities occurred. This included many instances with Arase, CASSIOPE, and NOAA/METOP. A brief campaign of transmissions during conjunctions with Van Allen Probe A was conducted before its end of mission in October 2019. Transmissions for VPM occurred during the period that satellite was in nominal operations, March–September 2020. The campaign with BARREL lasted January–March 2020. Three campaigns with FIREBIRD 4 were conducted in October–November 2020, January–March 2021, and May 2021. Table 4 provides counts of successful transmissions for these joint experiments.

Other than these specific WPIx transmission experiment campaigns, most experiments were relatively continuous throughout the mission. This includes passive collection of particle, wave, and environment effects data. An exception are the ACE experiments which were conducted in July 2019, January 2021, and March–May 2021.

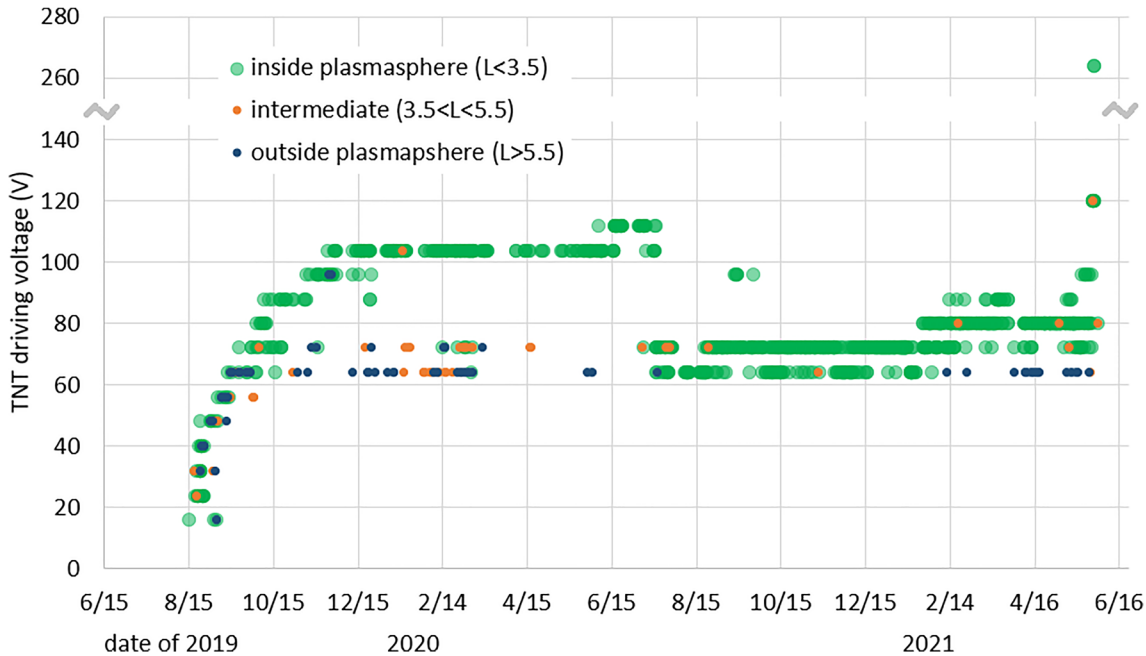


Figure 4. TNT driving voltage versus time for successful transmission data collection events with color indicating *L* value range.

Just prior to mission end, the "Hail Mary" campaign was completed, including successful completion of 9 out of 9 transmission DCEs at 120 V driving voltage (five in asymmetric mode and four in symmetric mode) and 2 out of 4 at 264 V (both successful ones were in asymmetric mode). Two final high-power transmits at 80 V on 31 May affirmed that TNT was still functioning nominally.

5.2. Data Collection

For the primary experiment, TNT successfully performed and acquired data for 1,338 high power transmission DCEs over the course of the mission with a total duration of 28,769 min. Planned transmission durations ranged from 10 to 40 min with an average of 21.5 min. Of transmission DCEs, 315 were in magnetic conjunction with other assets. TNT software and safeguards served well to manage expected and unexpected anomalies such that TNT continued operations through end of mission and achieved experiments at 264 V driving voltage in the final "Hail Mary" campaign. Figure 4 summarizes TNT high power transmission driving voltages versus time during the mission for successful DCEs, and Tables S1–S4 provide details for all transmission and receive DCEs. Two periods of frequent anomalies occurred. The first, in November 2019–January 2020, began with introduction of operations at 96 V and was eventually resolved with updated software. The second began in July 2020 and was managed with operations/programming changes.

BBR and VMAG survey data were collected throughout the mission. This included several BBR collects in which some or most payloads were turned off, allowing for high-sensitivity surveys of ambient waves. Comparison of results from early and late mission showed that BBR performance remained nominal throughout the mission. VMAG also performed well throughout the mission.

Five of the particle instruments each collected between 1 and 1.5 yr of data over the mission. Table 5 summarizes data collection by the particle instruments apart from HIPS (which failed at launch). The 9–25 September 2019 period (longer in some cases) with no data represents the first eclipse season where thermal and power management procedures were in development.

Two particle instruments failed and others showed suboptimal performance. As previously noted, HIPS failed at the start of the mission. LCI-HST had several brief periods of unphysical high background counts in some channels beginning in October 2019. It permanently failed on 3 November 2019 characterized by the same symptoms. In March 2020 CEASE began showing unphysical high counts in the two telescope channels observing low

21699402, 2023, 4, Downloaded from https://agupubs.onlinelibrary.wiley.com/doi/10.1029/2022JA030771 by Koc University, Wiley Online Library on [19/02/2025]. See the Terms and Conditions (https://onlinelibrary.wiley.com/terms-and-conditions) on Wiley Online Library for rules of use; OA articles are governed by the applicable Creative Commons License

21699402, 2023, 4, Downloaded from https://agupubs.onlinelibrary.wiley.com/doi/10.1029/2022JA030771 by Koc University, Wiley Online Library on [19/02/2025]. See the Terms and Conditions (https://onlinelibrary.wiley.com/terms-and-conditions) on Wiley Online Library for rules of use; OA articles are governed by the applicable Creative Commons License

Table 5
Data Collection by Demonstration and Science Experiments (DSX) Particle Instruments

Payload	File days[a]	Data days[b]	Start (UT)	Stop (UT)	Large data gaps (>7 days)
CEASE	562.0	552.0	13 August 2019 21:09	31 May 2021 17:15	09 September to 16 October 2019
LEESA	429.0	<427.6	29 July 2019 21:12	31 May 2021 15:15	09 September to 02 October 2019, 25 February to 12 March 2020, 12–23 July 2020
LIPS	588.7	558.8	29 July 2019 21:34	31 May 2021 17:15	09–25 September 2019
HEPS	417.9	408.6	13 August 2019 20:01	31 May 2021 07:11	15–27 August 2019, 07 September to 17 October 2019, 05–13 March 2020, 17–25 November 2020
LCI-FSH	394.8	<387.4	30 July 2019 20:47	31 May 2021 12:48	09–26 September 2019, 10–17 January 2020, 17 February to 12 March 2020, 24 June–03 July 2020, 29 September to 11 October 2020, 09 December 2020 to 14 January 2021, 18 January to 10 February 2021, 05–19 May 2021
LCI-HST	378.4	<54.2	30 July 2019 20:47	03 November 2019 19:46	09–26 September 2019

[a]File days represent time periods spanned by data files. [b]Data days represent cumulative time periods of valid data.

energy electrons, with these channels fully saturated by May 2020. Other telescope channels showed periods of high instrument background later in the mission, whereas dosimeter channels maintained normal performance. LIPS electron channels do not show expected behavior in comparison to CEASE channels of corresponding energy. Calibration work is ongoing, but at this time it appears that LIPS did not provide useful data at the designed energy ranges for electrons.

5.3. Notable Results

Here, we summarize some of the DSX science results and data analysis to date. Estimates of antenna impedances and radiated power have been made from TNT current and voltage data using an equivalent circuit model calibrated with pre-launch measurements. Values have been computed from data spanning the full VLF range over the entire mission and compared with predictions from several different cold-plasma electromagnetic wave propagation models. Results are described in Song et al. (2022) and Tu et al. (2023).

A large number of Blind Transmit DCEs (936) were conducted to explore the magnetospheric response to pulsed VLF transmissions. Whistler mode radio sounding from IMAGE demonstrated that depending on the wave frequency and initial wave normal angle, a VLF signal may bounce (echo) back to the transmitter by four distinct propagation paths (Sonwalkar et al., 2011; Sonwalkar, Reddy, & Carpenter, 2011). These four paths include signals that have: (a) magnetospherically reflected (Kimura, 1966), called boomerang mode (Edgar, 1972) or MR echo (Sonwalkar et al., 2011; Sonwalkar, Reddy, & Carpenter, 2011), (b) specularly reflected (Helliwell, 1965) at the Earth-ionosphere boundary (~90 km) at oblique incidence, called OI-SR echo, or (c) at normal incidence, called NI-SR echo (Sonwalkar et al., 2011; Sonwalkar, Reddy, & Carpenter, 2011), and (d) propagated in plasmaspheric ducts (Sonwalkar et al., 2004). Ray tracing calculations showed that signal return to DSX was expected following paths similar to those observed by IMAGE/RPI (Sonwalkar & Reddy, 2019). The potential also exists for signal amplification or triggered emissions via linear (Liemohn, 1967) or nonlinear processes (Li et al., 2015). Several of these phenomena were in fact observed. The top panel of Figure 5 shows an example of a boomerang detection: following the DSX transmission of a stepwise series of pulses, delayed return echoes are seen for each pulse ~0.5 s later. An apparent triggered emission is shown in the bottom panel of Figure 5. Here, the DSX transmission with pulses descending in frequency was followed by typical boomerang return signals near 22:57:22.5 UT, but then a rising frequency signal followed with duration ~1 s. For further discussion see Lauben et al. (2020) and Starks et al. (2022).

On 4 September 2019, DSX conducted high-power transmissions during a conjunction within 410 km spatial separation from Arase, using a transmission pattern crafted for a distinctive signal. Arase detected this signal at a range of ~1,100 km, while the two spacecraft were close to the same magnetic field line, but did not detect it at the

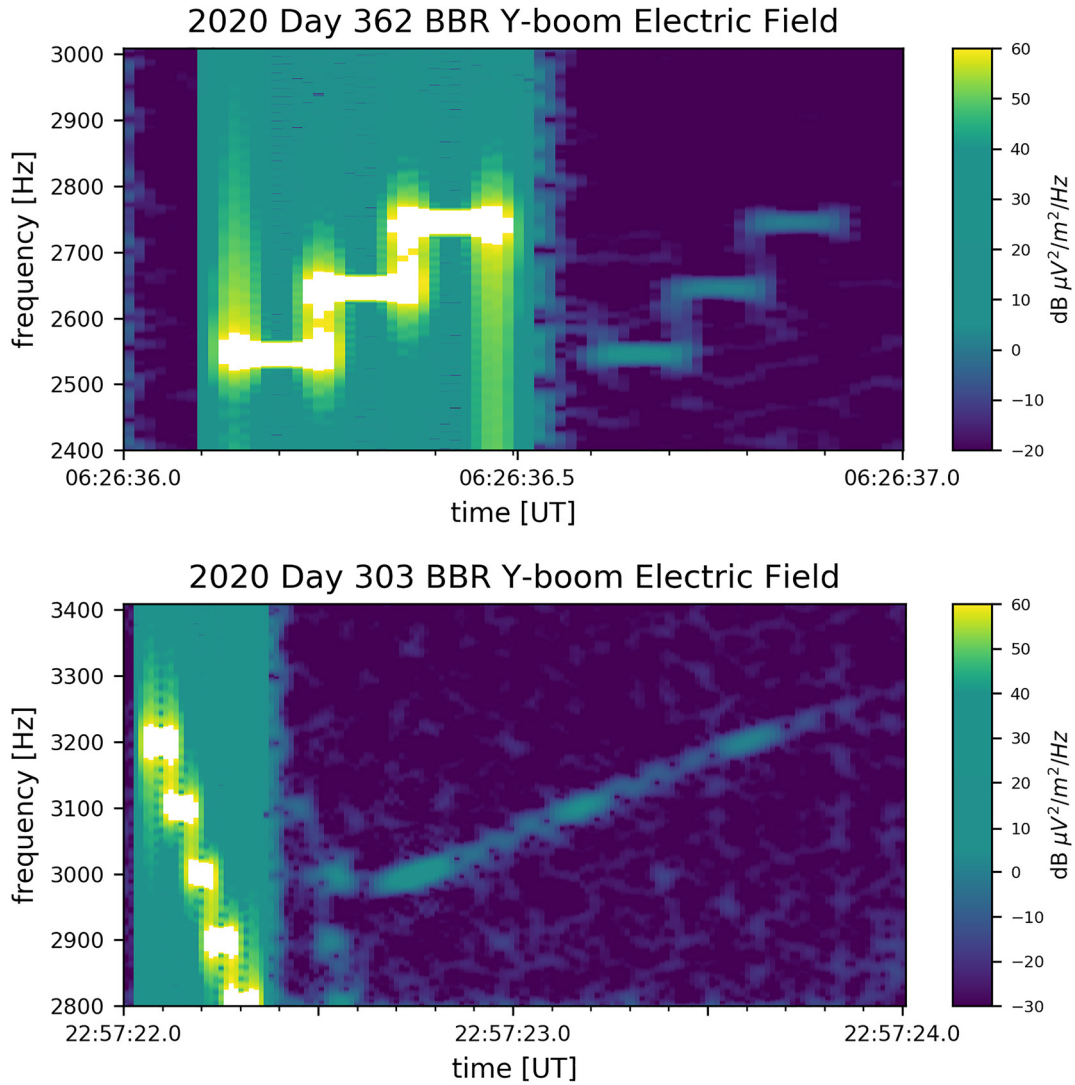


Figure 5. Spectrograms of BroadBand Receiver (BBR) observations from two data collection events showing Demonstration and Science Experiments (DSX) transmitted pulses and return signals. In each panel, electric field signals received on the *Y* antenna are shown with color mapped to a dynamic range of 90 dB and white regions during transmission of pulses represent saturation in the color map, not in BBR's dynamic range. Top panel shows a three-step pulse transmission on 27 December 2020 followed by detection of "boomerang echoes" or signals received back to DSX at 06:26:36.7–36.9 UT following remote reflection. Bottom panel shows a five-step pulse transmission on 29 October 2020 followed by typical boomerang echoes near 22:57:22.5 UT, then a triggered emission of ascending frequency at 22:57:22.7–23.8 UT.

time of closest spatial approach, in agreement with established theory that whistler waves in the magnetosphere propagate primarily along magnetic field lines (Helliwell, 1965). This marks the first confirmed space-to-space VLF transmission. Results are described in McCollough et al. (2022). Additional DSX-Arase conjunction results are under analysis.

DSX observed at least 45 episodes of whistler mode quasi-periodic (QP) emissions in the plasmasphere. QP emissions are previously described in the literature typically at 1–4 kHz, but DSX observed events include some as high as 15 kHz. Another unusual type of whistler mode emission observed by DSX included episodes with individual "up-drifting" (increasing in frequency) events overlapping each other in time. Results are described in Farrell et al. (2022).

Though multiple DSX transmissions were conducted while in conjunction with VPM, VPM data do not shown any signals attributable to DSX. These negative results further constrain the potential antenna pattern and field-aligned nature of VLF propagation. Results are described in Reid et al. (2022).

21699402, 2023, 4, Downloaded from https://agupubs.onlinelibrary.wiley.com/doi/10.1029/2022JA030771 by Koc University, Wiley Online Library on [19/02/2025]. See the Terms and Conditions (https://onlinelibrary.wiley.com/terms-and-conditions) on Wiley Online Library for rules of use; OA articles are governed by the applicable Creative Commons License

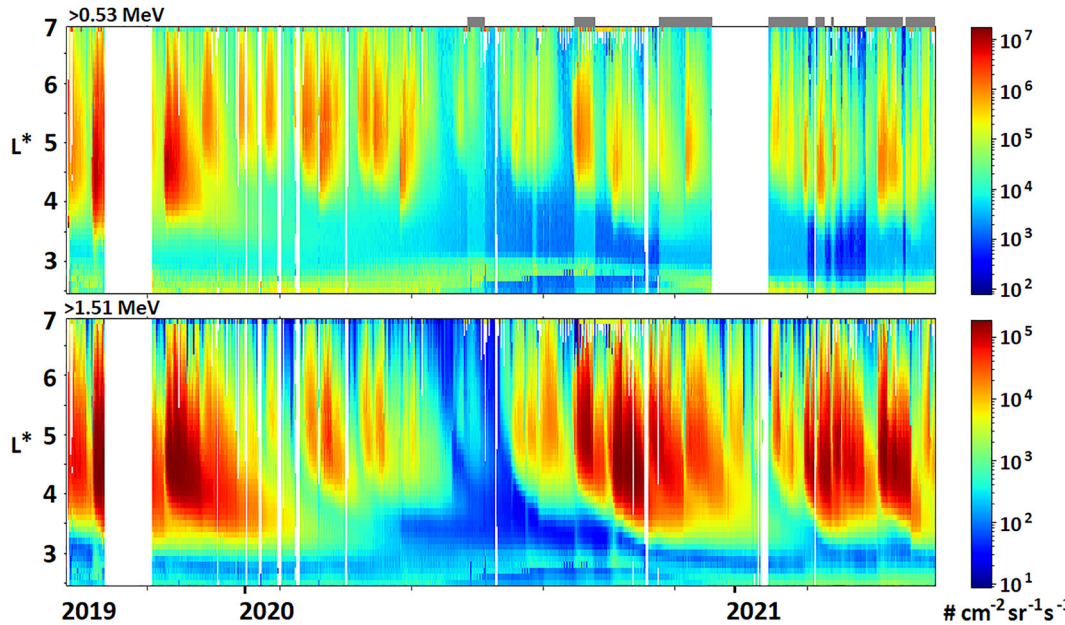


Figure 6. Compact Environmental Anomaly Sensor observations of electron fluxes during the Demonstration and Science Experiments mission versus time and L value for energies >0.53 MeV (telescope channel 04, top) and >1.51 MeV (dosimeter channel 07, bottom). Time periods of high instrument background in the telescope channel are indicated by gray bars at the top of the upper panel; the dosimeter channel is unaffected. Data are averaged in bins of 1 day and 0.1 in L*.

Calibration work is ongoing for most of the particle instruments. Figure 6 summarizes CEASE electron observations over the mission versus time and L value. The results show multiple episodes of outer belt dynamics despite being at solar minimum conditions. Features at $L^* < 3$ are proton contamination with apparent changes over time reflecting changes in DSX magnetic latitude sampling rather than proton belt changes. Instrumental issues account for the higher background fluxes in the >0.53 MeV channel at $L^* = 3$–4 after mid 2020. Spectral inversion of CEASE proton data to April 2020 has been conducted, showing good agreement with IRENE-AP9 climatology. Preliminary HEPS results also show agreement within a factor of 2 of IRENE-AP9 climatology.

Initial SET results include findings from the ELDRS experiment, representing the first tests for ELDRS effects in bipolar junction transistors. These results correlate well to ground-based studies and are described in Benedetto et al. (2021).

The first ACE experiments in July 2019 collected data for system identification of the spacecraft's flexible-body dynamics. The results of these experiments allowed for verification of boom deployment by comparing observed vibration modes against prelaunch predictions, but also demonstrated that the prelaunch predictions were not sufficiently accurate for high-bandwidth controller design (Davis & Sinclair, 2020). Experiments with controllers designed using the on-orbit identified model were conducted in March–May 2021. These results demonstrated bandwidth increase of 37x for the X axis, 7.5x for the Y axis, and 93.8x for the Z axis, relative to the nominal ADCS used throughout the mission. The results also demonstrated attenuation of five flexible modes by up to 15 dB.

5.4. Data Release Plans

DSX data sets will be released as calibration and quality control work is completed. They will be available at the NASA Space Physics Data Facility with first releases expected in the summer of 2023 and further releases over the next 1–2 yr as data sets are qualified for release. Generally, data levels for DSX payloads are produced as Level 0 (L0), comprising data sets of unprocessed instrument data (in payload/engineering units, raw counts, etc.) with associated ephemeris data; and Level 1 (L1), comprising calibrated data sets in scientific units associated

21699402, 2023, 4, Downloaded from https://agupubs.onlinelibrary.wiley.com/doi/10.1029/2022JA030771 by Koc University, Wiley Online Library on [19/02/2025]. See the Terms and Conditions (https://onlinelibrary.wiley.com/terms-and-conditions) on Wiley Online Library for rules of use; OA articles are governed by the applicable Creative Commons License

21699402, 2023, 4, Downloaded from https://agupubs.onlinelibrary.wiley.com/doi/10.1029/2022JA030771 by Koc University, Wiley Online Library on [19/02/2025]. See the Terms and Conditions (https://onlinelibrary.wiley.com/terms-and-conditions) on Wiley Online Library for rules of use; OA articles are governed by the applicable Creative Commons License

with extended ephemeris data. Both L0 and L1 data are planned for release. In addition to payload data, the L1 Extended Ephemeris (L1EE) daily files include:

- satellite ephemeris (day, time, orbit number, and location in cartesian, geodetic, and magnetic coordinates);
- satellite operations data (spacecraft attitude, high power transmit and torque rod flags, and DCE schedule);
- space environment data (IGRF magnetic field parameter, lightning flash rate at the footprints based on climatology [Colman, 2011], output from plasma density models (Carpenter & Anderson, 1992; Denton et al., 2004; and IRENE-SPM [Ginet et al., 2013]), plasmapause flag, and geomagnetic activity indexes); and
- conjunctions (satellite, transmitter, and lightning climatology [Colman, 2011]).

A single data format, Unified Measurement Storage (UMS), is the native format used for TNT L0 data. UMS files are accepted by the UML TNT Browser data visualization software to produce quick-look displays that include (a) high-power transmission voltage spectrogram; (b) passive reception dynamic spectrogram; and (c) relaxation sounding plasmagram. The plasmagrams provide visualization of sounding mode received signals in frequency and range (echo propagation delay time); for more discussion see Reinisch et al. (2000). A TNT converter is being developed to translate the data files from the UMS format into ASCII format so that other processing software can be used.

While the BBR raw data had a rate of 8 Mbit/s (~20 GB/orbit), they were processed on-board by SRx yielding downloaded data products of several hundred Mbytes/orbit. The SRx generated two continuous Survey products (SVY, Survey Spectrogram, MBA, Multiband Analyzer) and three on-demand Burst products (TPK, Time-Domain Packed, FPK, Frequency Domain Packed, and NBD, Narrowband). From the telemetry, each product generated L0 data in HDF format and quick-look graphics. The L1 processing code is under development.

The VMAG L1 data files in ASCII format contain time, position, magnetic parameter, altitude, high-power transmit flag, and three instrument directions and three magnetic field components in ECI coordinates.

Particle instrument L1 files generally include time, position, magnetic parameters, high-power transmit flag, pitch angle of instrument/pixel boresight, and fluxes for each energy channel and each species. Fluxes for standard channels are provided in the L1 files, while L0 files provide raw counts for these channels along with (for relevant payloads) additional logic bins.

5.5. DSX DCE Catalog

We provide as Supporting Information S1 a catalog of DSX DCEs. This DCE Catalog covers all scheduled DSX high-power VLF transmission and receive experiments including information such as time, physical and geomagnetic location, and transmission characteristics. The catalog data will support investigators seeking to identify DSX signals in other VLF observational data sets.

The catalog provides a listing of 2,150 successful or attempted DCEs (transmit or receive). Text and Figure S1 in Supporting Information S1 provide additional background on the DCE planning process. For each DCE Table S1 provides a unique identifier, summary of available data, DCE start/stop time and duration, instrument settings including TNT voltage and frequency, DSX attitude, type of experiment, conjunction information where applicable, and geomagnetic environment. Also included is each DCE's Joint Schedule identifier (JSID), which associates the DCE with planned settings for TNT and other payloads. For conjunctions with other satellites Table S2 provides additional information on the timing and duration of each conjunction plus spatial and geomagnetic locations of both DSX and the target satellite with their spatial and geomagnetic separations. For conjunctions with ground VLF transmitters, timing and duration of each conjunction is provided in Table S3. Table S4 summarizes types of science experiments including descriptive names, transmission pattern summary, and linkage to JSIDs. Table S5 identifies acronyms used in the catalog.

6. Conclusions

The DSX satellite operated for over 21 months successfully transmitting high-power VLF pulses into the Earth's magnetosphere and gathering a wealth of data on natural and artificial VLF emissions and in situ plasma and energetic particle populations. The 6,000 km × 12,000 km, 42° inclination orbit spanned the slot region and provided unique coverage that complements the traditional near-equatorial GTO radiation belt missions. In addition to the

21699402, 2023, 4, Downloaded from https://agupubs.onlinelibrary.wiley.com/doi/10.1029/2022JA030771 by Koc University, Wiley Online Library on [19/02/2025]. See the Terms and Conditions (https://onlinelibrary.wiley.com/terms-and-conditions) on Wiley Online Library for rules of use; OA articles are governed by the applicable Creative Commons License

usual challenges facing space missions, the planning and execution of active high-power experiments in a rarely visited orbital regime demanded a high level of personnel involvement which consumed much of the satellite operators', engineers' and project scientists' time during the mission itself. Pre-mission plans for many complex operating modes and near-real time processing turned out to be overly ambitious given the project resources and long delay time (over 16 yr) between spacecraft design, integration, and launch. Nevertheless, changes were made, processes streamlined and the tremendous amount of data collected more than meets the mission objectives. As analysis progresses, new scientific insights and practical applications can be expected regarding in situ VLF antenna radiation efficiency, far-field propagation, signal amplification, triggered emissions, and natural wave and particle populations in the MEO regime.

Data Availability Statement

Information regarding DSX Data Collection Events is provided in Supporting Information S1. Additional DSX data used to produce the figures is accessible at https://zenodo.org/record/7747383. Full DSX mission data will become available when post-mission processing and quality control is completed via the NASA Space Physics Data Facility.

Acknowledgments
The authors acknowledge Y.-J. Su, K. E. Carey, C. M. Straight, E. A. Kent, J. T. Langhals, S. A. Mendoza, B. Ryder, the DSX Operations Cadre and Mission Planning Team, and the Space Systems Command satellite operators for their roles in the mission. The authors thank J. S. Christmas, R. K. Delaney, M. R. Scherbarth, and J. A. Fennelly for program support. The authors also thank S. M. O'Malley, I. Vlad, A. G. Ling, and C. J. Roth of Atmospheric and Environment Research, Inc., for support of the DSX Data Center. DSX launch integration services and 1 year of on-orbit operations were provided by the Space Test Program at Space Systems Command and the authors acknowledge M. Marlow as STP-2 mission manager. DSX research and extended mission operations were funded by the Air Force Research Laboratory. NASA TASC development and data analysis at GSFC was funded by AFRL. University of Massachusetts Lowell work on TNT was supported by AFRL contracts FA8718-05-C-0027, FA9453-10-C-0220, and FA9453-18-C-0056. Stanford University work on BBR was supported by AFRL contracts FA8718-05-C-0027, FA9453-10-C-0220, and FA9453-18-C-0057. MIT-LL was supported by AFRL via AFLCMC contract FA8702-15-D-0001. J. Albert, W. R. Johnston, and M. J. Starks were supported by AFOSR Grant 22RVCOR002. S. L. Huston was supported by AFRL contract FA9453-19-C-0400. C. W. Parker was supported by AFRL contract FA9453-19-F-0003. The authors thank two anonymous reviewers for their constructive comments. The views expressed are those of the authors and do not reflect the official guidance or position of the United States Government, the Department of Defense or of the United States Air Force. The appearance of external hyperlinks does not constitute endorsement by the United States Department of Defense (DoD) of the linked websites, or the information, products, or services contained therein. The DoD does not exercise any editorial, security, or other control over the information you may find at these locations.

References

Abel, B., & Thorne, R. M. (1998). Electron scattering loss in Earth's inner magnetosphere: 1. Dominant physical processes. *Journal of Geophysical Research: Space Physics*, *103*(A2), 2397–2407. https://doi.org/10.1029/97JA02920

Baker, D. N., & Blake, J. B. (2012). SAMPEX: A long-serving radiation belt sentinel. In *Dynamics of the Earth's radiation belts and inner magnetosphere*, *Geophysical Monograph Series* (p. 199). American Geophysical Union. https://doi.org/10.1029/2012GM001368

Benedetto, A. R., Barnaby, H. J., Cook, C., Campola, M. J., & Tender, A. (2021). BJTs in space: ELDRS experiment on NASA Space Environment Testbed. *2021 IEEE Radiation Effects Data Workshop* (pp. 1–5). REDW. https://doi.org/10.1109/NSREC45046.2021.9679350

Brautigam, D. H. (2002). CRRES in review, space weather, and its effects on technology. *Journal of Atmospheric and Solar-Terrestrial Physics*, *64*(16), 1709–1721. https://doi.org/10.1016/S1364-6826(02)00121-9

Brautigam, D. H. (2008). Compact Environmental Anomaly Sensor (CEASE): Geometric factors (AFRL Report AFRL-RV-HA-TR-2008-1129). DTIC #ADA514447.

Burch, J. L. (2000). IMAGE mission overview. *Space Science Reviews*, *91*(1/2), 1–14. https://doi.org/10.1023/A:1005245323115

Carlsten, B. E., Colestock, P. L., Cunningham, G. S., Delzanno, G. L., Dors, E. E., Holloway, M. A., et al. (2019). Radiation-belt remediation using space-based antennas and electron beams. *IEEE Transactions on Plasma Science*, *47*(5), 2045–2063. https://doi.org/10.1109/TPS.2019.2910829

Carpenter, D. L., & Anderson, R. R. (1992). An ISEE/whistler model of equatorial electron density in the magnetosphere. *Journal of Geophysical Research*, *97*(A2), 1097–1108. https://doi.org/10.1029/91JA01548

Carpenter, D. L., Sonwalkar, V. S., Helliwell, R. A., Walt, M., Inan, U. S., Ikeda, M., & Caudle, D. L. (1997). Probing properties of the magnetospheric hot plasma distribution by whistler mode wave injection at multiple frequencies: Evidence of spatial as well as temporal wave growth. *Journal of Geophysical Research: Space Physics*, *102*(A7), 14355–14362. https://doi.org/10.1029/96JA03046

Carssow, D. B., Sullivan, J. D., Voss, D. L., Parker, C. W., Mavretic, A., Fritz, T. A., & Hubbard, A. E. (2009). Loss Cone Imager digital system design. In S. Fineschi, & J. A. Fennelly (Eds.), *Solar physics and space weather instrumentation III*, *Proceedings of the SPIE* (Vol. 7438, p. 743809). https://doi.org/10.1117/12.827374

Colman, J. J. (2011). Constructing a climatology of whistler wave energy from lightning in low earth orbit (AFRL report ARL-RV-PS-TR-2012-0055).

Davis, L. D., & Sinclair, A. J. (2020). Demonstration and Science Experiment Adaptive Control Experiment plan and preliminary system identification. *Advances in the Astronautical Sciences*, *175*, 713–722.

Denton, R. E., Menietti, J. D., Goldstein, J., Young, S. L., & Anderson, R. R. (2004). Electron density in the magnetosphere. *Journal of Geophysical Research: Space Physics*, *109*(A9), A09215. https://doi.org/10.1029/2003JA010245

Dichter, B. K., McGarity, J. O., Mullen, E. G., Brautigam, D. H., & Galica, G. E. (2009). Calibration of the High Energy Proton Spectrometer (HEPS) for the demonstration and Science Experiments (DSX) satellite space weather mission. In S. Fineschi, & J. A. Fennelly (Eds.), *Solar physics and space weather instrumentation III*, *Proceedings of the SPIE* (Vol. 7438, p. 743806). https://doi.org/10.1117/12.825647

Dichter, B. K., McGarity, J. O., Mullen, E. G., Brautigam, D. H., Galica, G. E., & Golightly, M. J. (2009). Calibration of the Compact Environmental Anomaly Sensor (CEASE) for the DSX space weather mission. In S. Fineschi, & J. A. Fennelly (Eds.), *Solar physics and space weather instrumentation III*, *Proceedings of the SPIE* (Vol. 7438, p. 743807). https://doi.org/10.1117/12.825665

Dichter, B. K., McGarity, J. O., Oberhardt, M. R., Jordanov, V. T., Sperry, D. J., Huber, A. C., et al. (1998). Compact Environmental Anomaly Sensor (CEASE): A novel spacecraft instrument for in situ measurements of environmental conditions. *IEEE Transactions on Nuclear Science*, *45*(6), 2758–2764. https://doi.org/10.1109/23.736525

Easley, S., Adler, A., Dichter, B. K., Ginet, G. P., Granata, J., Hausgen, P., et al. (2004). The AFRL DSX Flight Experiment. *Space 2004 Conference and Exhibit*. AIAA 2004-5892.

Edgar, B. C. (1972). *The structure of the magnetosphere as deduced from magnetospherically reflected whistlers* (Ph.D. dissertation). Stanford University.

Farrell, W. M., Lauben, D. S., Miller, J. A., Inan, U. S., Linscott, I. R., Galkin, I. A., et al. (2022). Quasi-periodic whistler mode emission in the plasmasphere as observed by the DSX spacecraft. *Journal of Geophysical Research: Space Physics*, *127*(8), e2022JA030327. https://doi.org/10.1029/2022JA030327

Fennelly, J. A. (2009). Demonstration and Science Experiment (DSX) Space Weather Experiment (SWx). In S. Fineschi, & J. A. Fennelly (Eds.), *Solar physics and space weather instrumentation III. Proceedings of the SPIE* (Vol. 7438, p. 743805). https://doi.org/10.1117/12.828321

Fowler, K. R., Frank, L. J., & Williams, R. L. (2004). Space Environment Testbed (SET): Adaptable system for piggybacked satellite experiments. *IEEE Transactions on Instrumentation and Measurement*, *53*(4), 1065–1070. https://doi.org/10.1109/TIM.2004.831497

Ginet, G. P. (2020). VLF far-field radiation from a linear dipole antenna immersed in a plasma: Baseline model for DSX (MIT-Lincoln Laboratory Report 95-0002). DTIC #AD1103378.

Ginet, G. P., O'Brien, T. P., Huston, S. L., Johnston, W. R., Guild, T. B., Friedel, R., et al. (2013). AE9/AP9/SPM: New models for specifying the trapped energetic particle and space plasma environment. *Space Science Reviews*, *179*(1–4), 579–615. https://doi.org/10.1007/s11214-013-9964-y

Golkowski, M., Harid, V., & Hosseini, P. (2019). Review of controlled excitation of nonlinear wave-particle interactions in the magnetosphere. *Frontiers in Astronomy and Space Sciences*, *6*, 2. https://doi.org/10.3389/fspas.2019.00002

Gombosi, T. I., Baker, D. N., Balogh, A., Erickson, P. J., Huba, J. D., & Lanzerotti, L. J. (2017). Anthropogenic space weather. *Space Science Reviews*, *212*(3–4), 985–1039. https://doi.org/10.1007/s11214-017-0357-5

Helliwell, R. A. (1965). *Whistlers and related ionospheric phenomena*. Stanford University Press.

Helliwell, R. A. (1988). VLF wave stimulation experiments in the magnetosphere from Siple Station, Antarctica. *Journal of Geophysical Research: Space Physics*, *26*(3), 551–578. https://doi.org/10.1029/RG026i003p00551

Helliwell, R. A., & Katsufrakis, J. P. (1974). VLF wave injection into the magnetosphere from Siple Station, Antarctica. *Journal of Geophysical Research*, *79*(16), 2511–2518. https://doi.org/10.1029/JA079i016p02511

Helliwell, R. A., Katsufrakis, J. P., & Trimpi, M. L. (1973). Whistler-induced amplitude perturbations in VLF propagation. *Journal of Geophysical Research*, *78*(22), 4679–4688. https://doi.org/10.1029/JA078i022p04679

Imhof, W. L., Reagan, J. B., Voss, H. D., Gaines, E. E., Datlowe, D. W., Mobilia, J., et al. (1983). Direct observation of radiation belt electrons precipitated by the controlled injection of VLF signals from a ground-based transmitter. *Geophysical Research Letters*, *10*(4), 361–364. https://doi.org/10.1029/GL010i004p00361

Johnson, A. T., Shumko, M., Griffith, B., Klumpar, D. M., Sample, J., Springer, L., et al. (2020). The FIREBIRD-II CubeSat mission: Focused investigations of relativistic electron burst intensity, range, and dynamics. *Review of Scientific Instruments*, *91*(3), 034503. https://doi.org/10.1063/1.5137905

Johnston, W. R., O'Brien, T. P., & Ginet, G. P. (2015). Release of AE9/AP9/SPM radiation belt and space plasma model version 1.20.002. *Space Weather*, *13*(6), 368. https://doi.org/10.1002/2015SW001212

Kanekal, S., Baker, D. N., & Sibeck, D. (2019). Recent advances in our understanding of the Earth's Radiation Belts. In *2019 International Conference on Electromagnetics in Advanced Applications (ICEAA)*. https://doi.org/10.1109/ICEAA.2019.8879310

Kennel, C. F., & Petschek, H. E. (1966). Limit on stably trapped particle fluxes. *Journal of Geophysical Research*, *71*, 1–28. https://doi.org/10.1029/JZ071i001p00001

Kimura, J. (1966). Effects of ions on whistler-mode ray tracing. *Radio Science*, *1*(3), 269–283. https://doi.org/10.1002/rds196613269

Lauben, D. S., Inan, U. S., Linscott, I. R., Galkin, I. A., Song, P., Stelmash, S., et al. (2020). Broadband reception of quasi-field-aligned "boomerang" echoes of in situ injected VLF pulses on the DSX spacecraft. In *Paper presented at AGU Fall Meeting 2020, abstract #SM016-03*.

Lehtinen, N. G., & Inan, U. S. (2009). Full-wave modeling of transionospheric propagation of VLF waves. *Geophysical Research Letters*, *36*(3), L03104. https://doi.org/10.1029/2008GL036535

Li, J. D., Spasojevic, M., & Inan, U. S. (2015). An empirical profile of VLF triggered emissions. *Journal of Geophysical Research: Space Physics*, *120*(8), 6581–6595. https://doi.org/10.1002/2015JA021444

Li, W., & Hudson, M. K. (2019). Earth's Van Allen radiation belts: From discovery to the Van Allen Probes era. *Journal of Geophysical Research: Space Physics*, *124*(11), 8319–8351. https://doi.org/10.1029/2018JA025940

Liemohn, H. B. (1967). Cyclotron-resonance amplification of VLF and ULF whistlers. *Journal of Geophysical Research*, *72*(1), 39–55. https://doi.org/10.1029/JZ072i001p00039

Lyons, L. R., & Thorne, R. M. (1973). Equilibrium structure of the radiation belt electrons. *Journal of Geophysical Research*, *78*(13), 2142–2149. https://doi.org/10.1029/JA078i013p02142

Mandell, M. J., Davis, V. A., McCollough, J. P., Johnston, W. R., Cooke, D. L., Wheelock, A. T., & Ferguson, D. C. (2019). *Nascap-2k modeling of electron and ion fluxes to DSX/LEESA during VLF transmission*. AIAA SciTech 2019 Forum, AIAA SciTech Forum. AIAA 2019-0312. https://doi.org/10.2514/6.2019-0312

Marshall, R. A., Sousa, A., Reid, R. A., Wilson, G. R., Starks, M. J., Ramos, D., et al. (2021). The Micro-Broadband Receiver (μBBR) on the very-low-frequency propagation mapper CubeSat. *Earth and Space Science*, *8*(11), e01951. https://doi.org/10.1029/2021EA001951

Mauk, B. H., Fox, N. J., Kanekal, S. G., Kessel, R. L., Sibeck, D. G., & Ukhorskiy, A. (2013). Science objectives and rationale for the Radiation Belt Storm Probes Mission. *Space Science Reviews*, *179*(1–4), 3–27. https://doi.org/10.1007/s11214-012-9908-y

McCollough, J. P., Miyoshi, Y., Ginet, G. P., Johnston, W. R., Su, Y.-J., Starks, M. J., et al. (2022). Space-to-space very low-frequency radio transmission in the magnetosphere using the DSX and Arase satellites. *Earth Planets and Space*, *74*(1), 64. https://doi.org/10.1186/s40623-022-01605-6

Michaels, D. (2011). Phaeton mast dynamics: On-orbit characterization of deployable masts. In *2011 Aerospace Conference* (pp. 1–10). https://doi.org/10.1109/AERO.2011.5747412

Millan, R. M., McCarthy, M. P., Sample, J. G., Smith, D. M., Thompson, L. D., McGaw, D. G., et al. (2013). The Balloon Array for RBSP Relativistic Electron Losses (BARREL). *Space Science Reviews*, *179*(1–4), 503–530. https://doi.org/10.1007/s11214-013-9971-z

Miyoshi, Y., Shinohara, I., Takashima, T., Asamura, K., Higashio, N., Mitani, T., et al. (2018). Geospace exploration project ERG. *Earth, Planets, and Space*, *70*(1), 101. https://doi.org/10.1186/s40623-018-0862-0

Moldwin, M. B. (2010). Vector Fluxgate Magnetometer (VMAG) development for DSX (AFRL Report AFRL-RV-HA-TR-2010-0156). DTIC #ADA529004.

Olson, W. P., & Pfitzer, K. A. (1974). A quantitative model of the magnetospheric magnetic field. *Journal of Geophysical Research*, *79*(25), 3739–3748. https://doi.org/10.1029/JA079i025p03739

Olson, W. P., & Pfitzer, K. A. (1977). Magnetospheric magnetic field modeling (Annual Scientific Report, AFOSR *Contract No. F44620-75-C-0033*).

Parker, C. W., Fritz, T. A., & Carssow, D. B. (2016). The Loss Cone Imager. *Nuclear Instruments and Methods in Physics Research, A*, *808*, 11–20. https://doi.org/10.1016/j.nima.2015.11.010

Parker, C. W., Sullivan, J. D., Coombs, J. M., Voss, D. L., Carssow, D. B., Mavretic, A., & Fritz, T. A. (2009). A high sensitivity telescope for measurements of energetic particles in the Earth's radiation belts. In S. Fineschi, & J. A. Fennelly (Eds.), *Solar physics and space weather instrumentation III*, *Proceedings of the SPIE* (Vol. 7438, p. 74380E). https://doi.org/10.1117/12.827375

Parker, C. W., Voss, D. L., & Fritz, T. A. (2014). Electron and proton beam testing of pixelated solid state detectors. *Nuclear Instruments and Methods in Physics Research, A*, *741*, 37–41. https://doi.org/10.1016/j.nima.2013.11.067

21699402, 2023, 4, Downloaded from https://agupubs.onlinelibrary.wiley.com/doi/10.1029/2022JA030771 by Koc University, Wiley Online Library on [19/02/2025]. See the Terms and Conditions (https://onlinelibrary.wiley.com/terms-and-conditions) on Wiley Online Library for rules of use; OA articles are governed by the applicable Creative Commons License

Paznukhov, V. V., Sales, G. S., Bibl, K., Reinisch, B. W., Song, P., Huang, X., & Galkin, I. A. (2010). Impedance characteristics of an active transmitting antenna radiating in the whistler mode. *Journal of Geophysical Research: Space Physics*, *115*(A9), A09212. https://doi.org/10.1029/2009JA014889

Reid, R. A., Marshall, R. A., Starks, M. J., Usanova, M. E., Wilson, G. R., Johnston, W. R., et al. (2022). Active VLF transmission experiments between the DSX and VPM spacecraft. *Journal of Geophysical Research: Space Physics*, *127*(4), e2021JA030087. https://doi.org/10.1029/2021JA030087

Reinisch, B. W., Haines, D. M., Bibl, K., Cheney, G., Galkin, I. A., Huang, X., et al. (2000). The Radio Plasma Imager investigation on the IMAGE spacecraft. *Space Science Reviews*, *91*(1/2), 319–359. https://doi.org/10.1023/A:1005252602159

Reinisch, B. W., Song, P., Galkin, I. A., Stelmash, S. S., Roche, K., Khmyrov, G. M., et al. (2022). The VLF transmitter, narrowband receiver, and tuner investigation on the DSX spacecraft. *Journal of Geophysical Research: Space Physics*.

Scherbarth, M., Adler, A., Smith, D., Loretti, V., & Stuart, J. (2009). AFRL's Demonstration and Science Experiments (DSX) mission. In S. Ryan (Ed.), *Proceedings of the Advanced Maui Optical and Space Surveillance Technologies Conference, held in Wailea, Maui, Hawaii, 1-4 September 2009* (p. E47). The Maui Economic Development Board.

Schoenberg, J., Ginet, G. P., Dichter, B., Xapsos, M. A., Adler, A., Scherbarth, M., & Smith, D. (2006). The Demonstration and Science Experiments (DSX): A Fundamental Science Research Mission Advancing Technologies that Enable MEO Spaceflight. Small Satellite System and Services, 20 September 2006, Italy.

Song, P., Reinisch, B. W., Paznukhov, V., Sales, G. S., Cooke, D. L., Tu, J.-N., et al. (2007). High voltage antenna-plasma interaction in whistler wave transmission: Plasma sheath effects. *Journal of Geophysical Research: Space Physics*, *112*(A3), A03205. https://doi.org/10.1029/2006JA011683

Song, P., Tu, J.-N., Galkin, I. A., McCollough, J. P., Ginet, G. P., Johnston, W. R., et al. (2022). Discovery and insights from DSX mission's high-power VLF wave transmission experiments in the radiation belts. *Scientific Reports*, *12*(1), 14304. https://doi.org/10.1038/s41598-022-18542-9

Song, P., Tu, J.-N., Reinisch, B. W., Galkin, I. A., & Johnston, W. R. (2021). Whistler mode radiation from a dipole antenna in cold magnetized plasma. *IEEE Transactions on Antennas and Propagation*, *70*(4), 2915–2927. https://doi.org/10.1109/TAP.2021.3121144

Sonwalkar, V. A., Reddy, A., & Carpenter, D. L. (2011). Magnetospherically reflected, specularly reflected, and backscattered whistler mode radio-sounder echoes observed on the IMAGE satellite: 2. Sounding of electron density, ion effective mass (m_{eff}), ion composition (H^+, He^+, O^+), and density irregularities along the geomagnetic field line. *Journal of Geophysical Research: Space Physics*, *116*(A11), A11211. https://doi.org/10.1029/2011JA016760

Sonwalkar, V. S., Carpenter, D. L., Bell, T. F., Spasojevic, M., Inan, U. S., Li, J., et al. (2004). Diagnostics of magnetospheric electron density and irregularities at altitudes <5,000 km using whistler and *Z* mode echoes from radio sounding on the IMAGE satellite. *Journal of Geophysical Research: Space Physics*, *109*(A11), A11212. https://doi.org/10.1029/2004JA010471

Sonwalkar, V. S., Carpenter, D. L., Helliwell, R. A., Walt, M., Inan, U. S., Caudle, D. L., & Ikeda, M. (1997). Properties of the magnetospheric hot plasma distribution deduced from whistler mode wave injection at 2,400 Hz: Ground-based detection of azimuthal structure in magnetospheric hot plasmas. *Journal of Geophysical Research: Space Physics*, *102*(A7), 14363–14380. https://doi.org/10.1029/96JA03047

Sonwalkar, V. S., Carpenter, D. L., Reddy, A., Proddaturi, R., Hazra, S., Mayank, K., & Reinisch, B. W. (2011). Magnetospherically reflected, specularly reflected, and backscattered whistler mode radio-sounder echoes observed on the IMAGE satellite: 1. Observations and interpretation. *Journal of Geophysical Research: Space Physics*, *116*(A11), A11210. https://doi.org/10.1029/2011JA016759

Sonwalkar, V. S., Inan, U. S., Bell, T. F., Helliwell, R. A., Molchanov, O. A., & Green, J. L. (1994). DE 1 VLF observations during Activny wave injection experiments. *Journal of Geophysical Research*, *99*(A4), 6173–6186. https://doi.org/10.1029/93JA03310

Sonwalkar, V. S., & Reddy, A. (2019). VLF/LF whistler mode wave injection and radio sounding experiments from the Demonstration and Science Experiments (DSX) satellite. In *Paper presented at AGU Fall Meeting 2019*. abstract #SM53A-07.

Starks, M. J., Albert, J. M., Johnston, W. R., Lauben, D. S., Linscott, I. R., Inan, U. S., et al. (2022). Understanding the VLF Bear Claw captured by the DSX spacecraft. In *Paper presented at the USNC-URSI National Radio Science Meeting 2022*. abstract #H2.1.

Starks, M. J., Albert, J. M., Ling, A. G., O'Malley, S., & Quinn, R. A. (2020). VLF transmitters and lightning-generated whistlers: 1. Modeling waves from source to space. *Journal of Geophysical Research: Space Physics*, *125*(3), e2019JA027029. https://doi.org/10.1029/2019JA027029

Sullivan, J. D. (2009). DSX loss cone imager differential response functions. In S. Fineschi, & J. A. Fennelly (Eds.), *Solar physics and space weather instrumentation III*, *Proceedings of the SPIE* (Vol. 7438, p. 74380A). https://doi.org/10.1117/12.825481

Thébault, E., Finaly, C. C., Beggan, C. D., Alken, P., Aubert, J., Barrois, O., et al. (2015). International Geomagnetic Reference Field: The 12th generation. *Earth, Planets, and Space*, *67*(1), 79. https://doi.org/10.1186/s40623-015-0228-9

Tu, J., Song, P., Galkin, I. A., Reinisch, B. W., Johnston, W. R., Starks, M. J., et al. (2023). Whistler mode transmission experiments in radiation belts: Circuit simulation and data analysis. *Journal of Geophysical Research: Space Physics*, *128*, e2022JA030564. https://doi.org/10.1029/2022JA030564

Voss, D. L., Gunda, A., Carssow, D., Fritz, T. A., Mavretic, A., & Sullivan, J. D. (2009). Overview of the loss cone imager fixed sensor head instrument. In S. Fineschi, & J. A. Fennelly (Eds.), *Solar physics and space weather instrumentation III*, *Proceedings of the SPIE* (Vol. 7438, p. 743808). https://doi.org/10.1117/12.825481

Winter, J., Spanjers, G., Cohen, D., Adler, A., Ginet, G. P., Dichter, B. K., et al. (2004). A proposed large deployable space structures experiment for high power, large aperture missions in MEO. In *2004 IEEE Aerospace Conference Proceedings* (pp. 525–532). https://doi.org/10.1109/AERO.2004.1367636

Yando, K., Millan, R. M., Green, J. C., & Evans, D. S. (2011). A Monte Carlo simulation of the NOAA POES medium energy proton and electron detector instrument. *Journal of Geophysical Research: Space Physics*, *110*(A10), A10231. https://doi.org/10.1029/2011JA016671

Yau, A. W., Ali, Z., Alonso, C., Casgrain, C., Enno, G. A., Entus, B., et al. (2015). The Canadian CASSIOPE small satellite mission: The enhanced polar outflow probe and Cascade technology demonstration payloads. *Acta Astronautica*, *110*, 155–160. https://doi.org/10.1016/j.actaastro.2015.01.016

References From the Supporting Information

Alken, P., Thébault, E., Beggan, C. D., Amit, H., Aubert, J., Baerenzung, J., et al. (2021). International Geomagnetic Reference Field: The thirteenth generation. *Earth, Planets, and Space*, *73*(1), 49. https://doi.org/10.1186/s40623-020-01288-x

Roth, C. (2017). *IRENE: AE9/AP9/SPM radiation environment model user's guide version 1.50.001*. Air Force Research Laboratory. Retrieved from https://www.vdl.afrl.af.mil/programs/ae9ap9/files/package/Ae9_Ap9_SPM_Users_Guide.pdf

21699402, 2023, 4, Downloaded from https://agupubs.onlinelibrary.wiley.com/doi/10.1029/2022JA030771 by Koc University, Wiley Online Library on [19/02/2025]. See the Terms and Conditions (https://onlinelibrary.wiley.com/terms-and-conditions) on Wiley Online Library for rules of use; OA articles are governed by the applicable Creative Commons License